Appendix Chapter 6d: Exploring the Effects of Changes in Tropospheric Ozone on UVB

Atmospheric ozone filters harmful solar ultraviolet radiation (UV-B), thereby reducing the amount of UV-B reaching the Earth's surface. The majority of ozone—about 90%—is located in the stratosphere, and the stratospheric ozone layer provides most of this protective filtration. Tropospheric ozone, located at ground level, accounts for the remaining 10% of atmospheric ozone. Although only a portion of ground level ozone can be attributed to anthropogenic sources, it is reasonable to assume that reducing ground level ozone would reduce the UV-B filtration provided, and thus would lead to increases in health effects normally associated with reductions in stratospheric ozone. UV radiation-induced health effects are primarily related to the skin (e.g., melanoma and nonmelanoma skin cancer), eyes (e.g., cataracts), and immune system.

The attached preliminary report entitled "Analysis of the Impact of Emissions Changes on Tropospheric Ozone" represents the EPA's first attempt to develop a methodology for capturing the changes in skin cancers and their economic value that might be associated with changes in tropospheric ozone. This initial effort was designed as a scoping analysis to determine the potential magnitude of impacts, and is not intended to serve as a standard methodology for assessing UVB impacts in future RIAs. This scoping analysis focuses on a scenario reflecting the likely distribution of ground level ozone in the Eastern United States domain under an illustrative set of controls intended to reduce ozone concentrations towards attainment of an ozone standard of 70 parts per billion (ppb), as compared to the current ozone National Ambient Air Quality Standard (NAAQS) for 2020.[1] The report only examines the effects of this reduced UV filtration on incidence of and mortality associated with skin cancers – specifically, basal cell carcinoma (BCC), squamous cell carcinoma (SCC) and cutaneous malignant melanoma (CMM).

The general methodology developed for this draft scoping analysis was applied in four steps. First, changes in ground level UV radiation (for geographical extent) were estimated using the Community Multiscale Air Quality model results as an input to the Tropospheric Ultraviolet – Visible radiation model (TUV). The CMAQ model runs provided data for each of 14 altitude layers for each location on a 12x12 km grid at hourly intervals for 24 hours of each day from June 1, 2020 to August 31, 2020. Using these data, the TUV model produced estimates of the daily integrated dose of UV exposure. Second, population-weighted exposure estimates were derived using county based population projections developed using a cohort-component methodology. Third, the resulting estimates were used in the Atmospheric Health Effects Framework model to quantify expected changes in incidence in and mortality from basal cell carcinoma (BCC), squamous cell carcinoma (SCC) and cutaneous malignant melanoma (CMM) associated with the given change in ground level ozone. Fourth, the resulting health effects were monetized using a combination of estimates of the value of statistical life and willingness to pay to avoid a case of skin cancer.

This research makes use of results from the CMAQ, TUV and AHEF models. These models have all been applied extensively in other contexts but this is their first application to estimate

[1] This scenario was developed for the Ozone NAAQS Proposal and does not match runs produced for the Ozone NAAQS Final.

skin cancer effects associated with changes in tropospheric ozone.[2] While all of these models have been extensively peer reviewed and validated in different contexts, the reviews were focused on different model applications and did not extend necessarily to the current problem.

We subjected this scoping analysis to peer review by five experts external to the Agency, including Dr. Edward DeFabo, George Washington University; Dr. Hugh Ellis, Johns Hopkins University; Dr. Scott Farrow, University of Maryland – Baltimore County; Dr. Randy Kawa, National Atmospheric Sciences Administration; and Dr. Helen Suh, Harvard School of Public Health.[3] Unfortunately, due to time constraints, we were unable to incorporate the recommendations from the reviewers in time for this rule. However, the Agency plans to respond to peer reviewer remarks in the near future as we continue our efforts on exploring this topic.

Although the draft report addresses a number of sources of uncertainty, we recognize that others may remain including, but not limited to, the applicability of epidemiologic studies of long-term UV-B exposures over broad geographic regions to scenarios involving impacts of smaller, more variable, localized changes in ground level ozone; the variation in activity patterns and other factors that determine population exposures and sensitivities to UV-B radiation; as well as the effects of aerosols. These uncertainties have been recognized by the Agency and discussed in Chapter 10 of the most recent Ozone Criteria Document (U.S. EPA, 2006). The Agency will consider whether to conduct additional exploratory analyses related to UVB screening as we continue our efforts to quantify health effects associated with reduced tropospheric ozone in a rigorous and defensible manner.

Because the CMAQ modeling runs used for this scoping analysis do not match those used for the Ozone NAAQS Final Regulatory Impact Assessment (RIA), direct comparisons of the monetized skin cancer effects associated with reduced UV-B filtration presented in this report cannot be made with health benefit results presented in the RIA for the final rule. Still, comparing the results of this scoping analysis with the estimates of benefits presented in the proposal RIA, provides a general sense of the order of magnitude of the resulting effects. The estimates of monetized disbenefits resulting from increased UVB levels due to reduced tropospheric ozone as captured by this scoping analysis amount to approximately 0.3 to 0.6 percent of the monetized health benefits associated with the modeled set of ozone precursor control strategies reported in the proposal RIA.

[2] TUV and AHEF were developed to estimate health effects associated with changes in stratospheric ozone.
[3] The individual reports from each of the peer reviewers are contained in the docket for this rule.

Analysis of the Impact of Emissions Changes on Tropospheric Ozone

DRAFT Report
February 18, 2008

Prepared by:

ICF International

Table of Contents

Introduction

Atmospheric ozone filters harmful solar ultraviolet radiation (UV-B), thereby reducing the amount of the UV-B reaching the Earth's surface. The majority of ozone—about 90%—is located in the stratosphere, and the stratospheric ozone layer provides most of this protective filtration. Tropospheric ozone, located at ground level, accounts for the remaining 10% of atmospheric ozone. Although only a portion of ground level ozone can be attributed to anthropogenic sources, it is reasonable to assume that reducing ground level ozone would reduce the UV-B filtration provided, and thus would lead to increases in health effects normally associated with reductions in stratospheric ozone. UV radiation-induced health effects are primarily related to the skin (e.g., melanoma and nonmelanoma skin cancer), eyes (e.g., cataracts), and immune system.

The purpose of this report is to assess these human health effects of reduced UV filtration associated with the reduction of ground level ozone under an ozone standard of 70 parts per billion (ppb) compared to the current ozone National Ambient Air Quality Standard (NAAQS) for 2020.

The remainder of this paper is organized as follows:

- Section 2 describes the methodology used to carry out this assessment, including modeling using the Tropospheric Ultraviolet-Visible radiation model (TUV) and the U.S. EPA's Atmospheric and Health Effects Framework (AHEF);
- Section 3 presents the results of the analysis, including changes in ground level UV and health effects; and
- Section 4 addresses the uncertainties associated with modeling undertaken for this analysis.

Methodology

1.1. CMAQ Modeling

The inputs for this analysis were generated through Community Multiscale Air Quality (CMAQ) ozone modeling runs. The CMAQ model produced spatial fields of gridded ozone concentrations on an hourly basis for the Eastern United States domain with 12 km horizontal resolution and 14 vertical layers topping out at 16,200 meters.

1.2. TUV Modeling

1.2.1. Tropospheric Ozone Scenarios

The CMAQ model provided ozone concentrations in parts per billion (ppb) for each of the 14 altitude layers given in Table 1. These values are specified for each location (latitude, longitude) on a 12 × 12 km grid (66920 locations) at hourly intervals for 24 hours (UT) of each day from 1

Jun to 31 Aug 2020. Two scenarios are considered with identifiers:
2020bk_v4.5_084_12km.o3_hr_shift_LST, and
2020bk_v4.5_070b_12km.o3_hr_shift_LST.
For brevity, these scenarios will be called 084 and 070, respectively.

In order to model a hypothetical control strategy incremental to attainment of the current standard (84 ppb), EPA approached the analysis in stages. First, EPA identified controls to be included in the baseline. These included current state and federal programs plus controls to attain the current ozone standard and PM2.5 PM standards (see http://www.epa.gov/ttnecas1/ria.html for a complete list of controls). Then, EPA applied additional known controls within geographic areas designed to bring areas predicted to exceed 70 ppb in 2020 into attainment (U.S. EPA, 2008).

Table 1 gives the vertical structure of the model. The 14 layers are bounded by 15 levels defined on unequally spaced modified normalized pressure coordinates (sigma = 1 at the surface, 0 at the top of the model). The actual atmospheric pressures, and corresponding geometric altitudes, are determined by the meteorological input to CMAQ and vary in time and space. Approximate values are given in the table. For the purposes of the radiative transfer calculations, the approximate heights given in Table 1 were used, and sensitivity calculations were made to bracket the effect of this approximation. The last column of Table 1 gives the number of air molecules, per square centimeter, in a vertical column within each layer, and their calculation is described in the following section.

Table 1: Vertical Structure for 14 Layer CMAQ (heights are the top of layer).

Layer Number	Sigma	Approximate Height (m)	Approximate Pressure (mb)	Air column between levels (molecules cm^{-2})
0	1.000	0	1000	—
1	0.995	38	995	9.67×10^{22}
2	0.990	77	991	9.89×10^{22}
3	0.980	154	982	1.94×10^{23}
4	0.960	310	964	3.89×10^{23}
5	0.940	469	946	3.90×10^{23}
6	0.910	712	919	5.85×10^{23}
7	0.860	1,130	874	9.73×10^{23}
8	0.800	1,657	820	1.17×10^{24}
9	0.740	2,212	766	1.17×10^{24}
10	0.650	3,108	685	1.75×10^{24}
11	0.550	4,212	595	1.95×10^{24}

Layer Number	Sigma	Approximate Height (m)	Approximate Pressure (mb)	Air column between levels (molecules cm^{-2})
12	0.400	6,153	460	2.91×10^{24}
13	0.200	9,625	280	3.85×10^{24}
14	0.000	15,674	100	3.58×10^{24}

The detailed CMAQ ozone values were used in the calculations of the UV radiation. However, to illustrate the magnitude of the changes in ozone, Figure 1 shows the concentration changes from the 084 to the 070 CMAQ scenarios, averaged over the entire geographic domain and over hours of all days of each month. Also shown are the values for 15 July (the mid-time of the simulation), since this date will be used in some sensitivity studies in Section 4.3. The largest changes are seen to occur between ca. 500 and 1000 m above the surface (layers 5–7, see Table 1) and are non-negligible even in the highest layers.

Figure 1: Domain-averaged ozone concentration changes (ppb) in each CMAQ layer. Vertically averaged changes (ppb) are given in the legend.

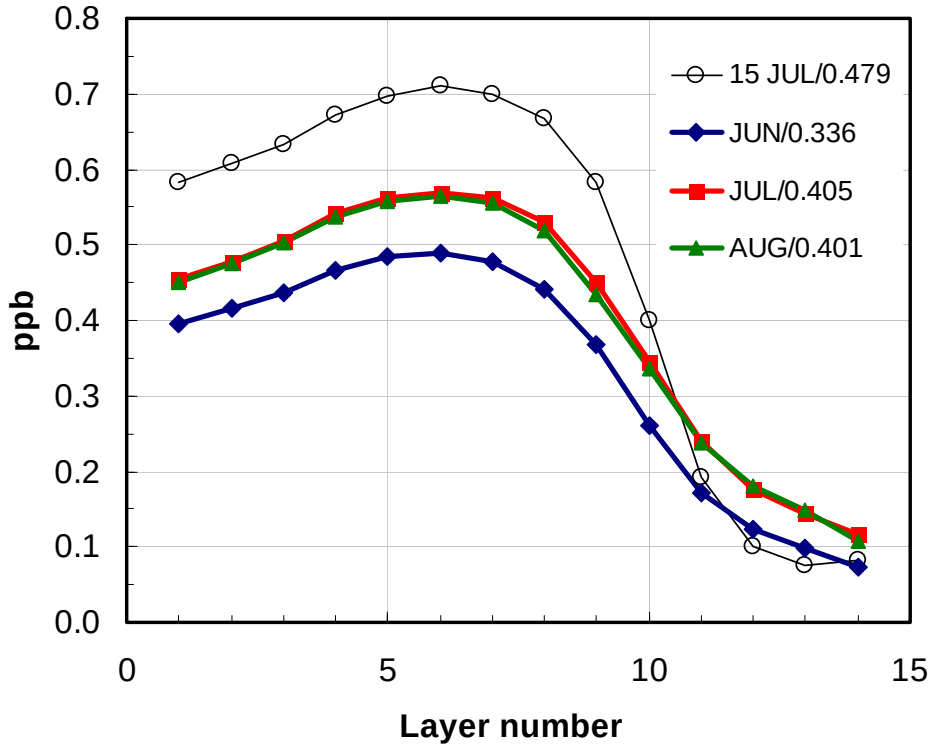

The contribution of each layer to the ozone column change is given in Figure 2. This was obtained by multiplying the concentration changes (ppb) by 10^{-9} times the air column in each

corresponding layer (from Table 1), and converting to Dobson Units (DU) by dividing by 2.687×10^{16} molecules cm^{-3} DU^{-1}. The total ozone column change is the sum of the contributions in each layer, and is shown in the figure legend. The small contribution from the lowest levels is due mainly to their small vertical thickness, while the decreasing contribution of the uppermost layers is due to the exponential decrease in air density with altitude. Notably, the highest contributions are from layers 7–10 (ca. 1–3 km altitudes), with non-negligible contributions from the upper troposphere as already noted above.

Figure 2: Domain-averaged ozone column changes (Dobson Units) in each CMAQ layer. The sum of the ozone changes (Dobson Units) is given in the legend, and is the total ozone column change.

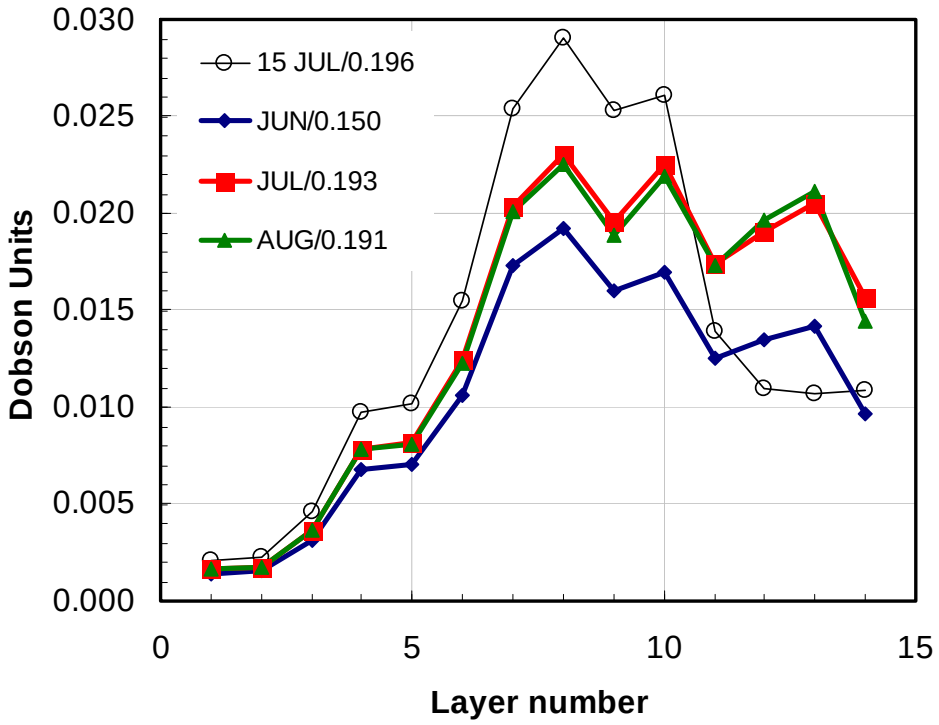

The ozone changes shown in Figures 1 and 2 cannot be translated directly into changes of surface UV radiation, because they are averaged over different locations and times. For example, they include night-time values when the UV radiation is non-existent. This can be seen in Table 2, where the domain-averaged ozone changes for 15 July were divided according to whether they occur for solar zenith angels (sza) smaller than 45 degrees (high sun) and lower than 45 degrees (low sun). The table shows that the changes in surface and column values are largest for high sun, consistent with photochemical formation near sources, and coincident with times of highest surface biologically active irradiances. Mid-tropospheric values have a weaker dependence on sza, consistent with long-range transport and a relatively long ozone lifetime.

Table 2: Ozone change statistics for 15 July 2020, CMAQ scenarios 084-070

		Number of points	Average ozone change (ppb) at surface	Average ozone change (ppb) at level 12 (~ 500 mb)	Average ozone column change, Dobson Units
All sza		1,605,600	0.58	0.10	0.20
sza < 45^o	high sun	426,139	0.69	0.11	0.22
45^o < sza < 90^o	low sun	538,529	0.60	0.09	0.19
sza > 90^o	night	640,932	0.50	0.11	0.19

An independent albeit rough estimate of the ozone column (DU) change can be obtained from the concentrations given in Table 2. Considering only the values for sza < 45^o (c.f., the simple rule that UV exposure should be avoided when a person's shadow is shorter than a person's height), even a simple linear average of the ozone changes at the surface and 500 mb yields ~ 0.4 ppb, and can be taken as applicable to the lower half of the atmosphere (below 500 mb). The total atmospheric column of air is about 2.0×10^{25} molecules cm^{-2}, so taking half of this and 0.4 ppb ozone yields 4×10^{15} molecules cm^{-2} of ozone ($1.0 \times 10^{25} \times 0.4 \times 10^{-9}$), or ≈ 0.15 Dobson Units. This is reasonably close to the column value in the table, 0.22 DU, which was calculated within TUV from the full vertical variation of ozone and air concentrations, and included changes above 500 mb as well as an exponential profile of air density which of course gives more weight to the lower altitudes.

1.2.2. TUV Model Calculations

The surface ultraviolet radiation was calculated with the Tropospheric Ultraviolet-Visible (TUV) model developed by Madronich and co-workers at the National Center for Atmospheric Research (NCAR). The TUV model is widely used for the calculation of atmospheric and surface UV radiation including international assessments of the environmental effects of stratospheric ozone depletion (e.g., Madronich et al., 1998), and has been evaluated in numerous model-measurement intercomparison studies (e.g., Koepke et al., 1998; Bais et al., 2003). An early version of TUV, of similar accuracy but lesser flexibility, is used within the CMAQ atmospheric chemistry module to compute photolysis frequencies. The model has been described in the literature (e.g., Madronich and Flocke, 1999) and the latest version (version 4.5, used here) is freely available to the scientific community through NCAR Community Data Portal (http://cdp.ucar.edu).

Several modifications to the TUV model were made for the present purposes, specifically to (i) interface the model with the CMAQ ozone concentrations, and (ii) to speed up the computational time in view of the large number of locations reported by the CMAQ model.

The altitude grid was modified to match the values given in Table 1, then continuing to 16 km and increasing by 2 km to 40 km, and by 5 km to 80 km. These represent altitude levels, while layers (to which the ozone concentrations are applied) are the volume between these levels. The TUV model used the U.S. Standard Atmosphere (USSA, 1976) vertical profiles of temperature

(K), air density and ozone (both molecules cm^{-3}), specified from sea level to 80 km in 1 km increments, and then interpolated to the altitude grid described above. Because the CMAQ model has layers that are both smaller and larger than the standard USSA 1 km grid, some attention was given to proper vertical interpolation of air density. Specifically, the logarithm of the USSA air number density (molecules cm^{-3}) was interpolated linearly to obtain the logarithm of the air density at the CMAQ levels. Then, the vertical air column (molecules cm^{-2}) of each layer was obtained by logarithmic integration:

$$\text{Air column in layer } k = dz\,[\,y(k+1) - y(k)\,] \,/\, \ln[\,y(k+1) \,/\, y(k)\,]$$

where $dz = z(k+1) - z(k)$ = vertical thickness of the layer. The air column of each layer was then multiplied by the CMAQ ozone concentrations (ppb $\times 10^{-9}$) to yield the ozone column in each layer (molecules cm^{-2}), so overwriting the USSA ozone values for these altitudes. For altitudes above the highest level of Table 1, the interpolated USSA ozone values were used.

For each wavelength interval (see below), the radiative transfer solution was expressed analytically using the delta-Eddington approximation (Joseph et al., 1976) formulated in generalized 2-stream equations (Toon et al., 1989) corrected for atmospheric curvature using a pseudo-spherical approximation (Petropavlovskih, 1995). The resulting set of coupled 2N equations (N = number of layers) was solved by tridiagonal matrix inversion to obtain the spectral irradiance, $I(\lambda)$ in W m^{-2} nm^{-1} for a given wavelength, time, and location. This calculation was repeated for the center of each wavelength interval, for each location, for each hour (on the half-hour) of each day of June, July, and August for each of the two given CMAQ scenarios. The spectral irradiance was multiplied by a biological sensitivity function (action spectrum) $B(\lambda)$, then integrated numerically all wavelengths with non-zero contributions, to obtain the surface biological exposure (biologically effective irradiance) I_{bio} (W m^{-2}). Two different action spectra were considered: (1) the CIE standard erythemal (skin-reddening) spectrum (McKinlay and Diffey, 1987) which forms the basis of the WMO/WHO-recognized UV Index computed operationally in the United States by NOAA and highlighted by the EPA, and (2) the spectrum for the induction of non-melanoma skin cancer in mice, corrected for human skin transmission (deGruijl and van der Leun, 1994). The latter spectrum has been used extensively in the assessments of ozone depletion, and is named SCUP-h (Skin Cancer Utrecht-Philadelphia, reflecting the location of the research groups that originated it), and its sensitivity to ozone changes is quite similar to that of the erythemal spectrum (as shown by Madronich et al., 1998). For brevity, biologically effective irradiances computed from these two spectra are hereafter called I_{ERY} and I_{SCUP}. Values of I_{SCUP} are used in ICF's AHEF model as measures of human exposure to UV radiation.

The TUV wavelength (nm) grid extended from 294 to 330 by 2 nm, to 350 by 5 nm, and to 400 by 10 nm. The higher resolution at the shorter wavelengths is required to represent accurately the absorption by ozone which is strongly dependent on wavelength, while the coarser resolution provides computational efficiency. A resolution of 2 nm in the ozone-dependent region has been show to be sufficiently accurate for photolysis calculations, including $O_3 + h\nu \rightarrow O_2 + O(^1D)$ which has a spectral dependence similar or steeper (and therefore more sensitive to spectral resolution) than the action spectra used here (Madronich and Weller, 1990).

For each location on the 12 × 12 km grid, the values of I_{ERY} and I_{SCUP} were integrated over 24 hours to provide daily integrated doses, and over each month (June, July, and August) to provide monthly integrated values. Otherwise identical calculations were performed for the 070 and 084 scenarios, and the difference between scenarios was computed for each location.

Tropospheric ozone causes a larger change, on a per molecule basis, than stratospheric ozone (Bruhl and Crutzen, 1989), at least for high sun. This is because of coupling between molecular (Rayleigh) scattering and ozone absorption: Scattering increases the tropospheric photon path lengths and therefore increases the probability of absorption by tropospheric absorbers including ozone. Figure 3 shows the normalized sensitivity of SCUP-h weighted UV as a function of the altitude where the ozone perturbation occurs. The normalized sensitivity (also called the Radiation Amplification Factor, RAF) is the % increase in radiation for each % decrease in ozone column. For this plot, a 1 DU of ozone was inserted in a 1 km layer at various altitudes (the altitudes of ozone perturbation in the figure), and the resultant surface UV-SCUP values compared to the reference calculation (without the 1 DU). The RAF is then:

$$\mathrm{RAF} = -\ln(UV_2/UV_1)/\ln(DU_2/DU_1)$$

where the subscripts 2 and 1 refer to the perturbed and reference calculations (Micheletti et al., 2003).

Figure 3: Normalized sensitivity (% for %) of UV-SCUP changes to the altitude at which ozone perturbations are made.

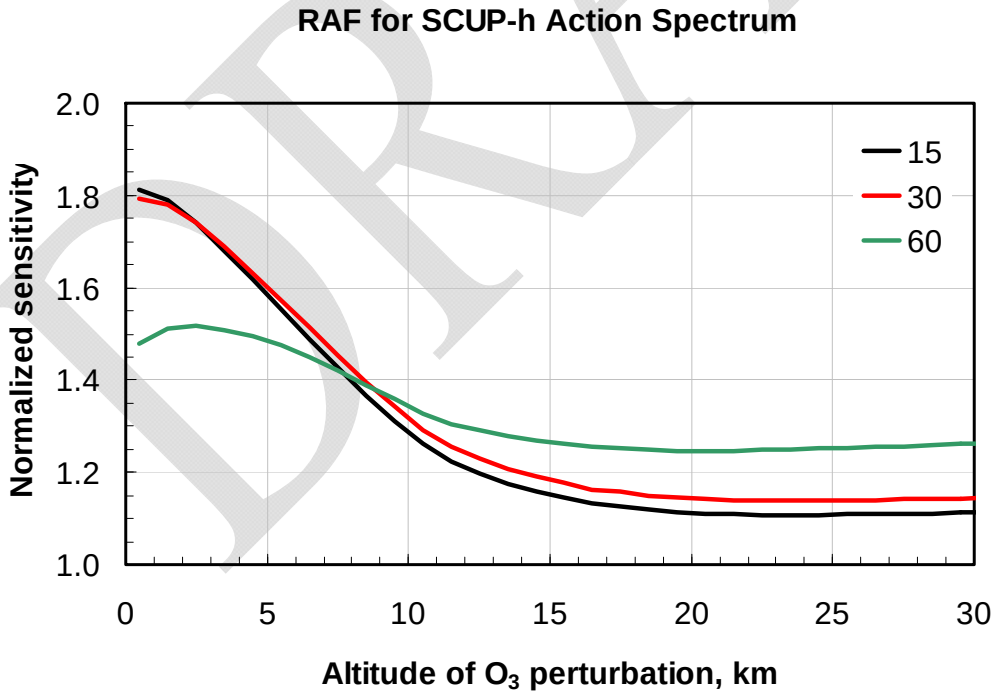

For example, a 0.22 DU increment (from Table 1, 15 July, high sun) represents about 0.06% change in the ozone column (349 DU for the USSA, but actually somewhat different and variable when using the CMAQ values up to 16 km). From Figure 3, a RAF of 1.6–1.7 is reasonable for ozone perturbations in the low-mid troposphere and relatively high sun when UV matters. Multiplying (0.06 % × 1.65), the surface UV-SCUP radiation is expected to change by about 0.1 %. This is the approximated magnitude of the UV-SCUP changes expected between the two CMAQ scenarios.

Of course, the full TUV calculations were done with high spectral resolution (not simple scaling with RAFs), time integration over actual sza values, full vertical distributions of tropospheric ozone given by the CMAQ, and fully coupled scattering-absorption multi-layer radiative transfer. Therefore they are expected to be more accurate, and more firmly anchored in the state-of-the-science.

1.2.3. TUV Results

Detailed maps of UV-SCUP distributions and percent changes are given in Appendix A. Here, the results are summarized in Figure 4 as domain-averaged UV-SCUP percent changes for each day. They range from 0.05 % to 0.16 %, with most values near 0.1 % or slightly higher (note that % changes of the monthly UV increments are not strictly equal to the monthly averages of daily % changes, though they happen to be quite similar). Figure 5 shows the frequency distribution of the monthly increments expressed as percent. The most common value is near zero, and few values above 0.3%. A few negative values were noted. Finally, it should be clear that the data in these figures are not yet weighted by the affected populations, and therefore should be viewed as changes in the physical state of the atmosphere, not as measures of population exposure.

Figure 4: Domain-averaged percent changes in SCUP-weighted daily doses changes between 070 and 084 scenarios

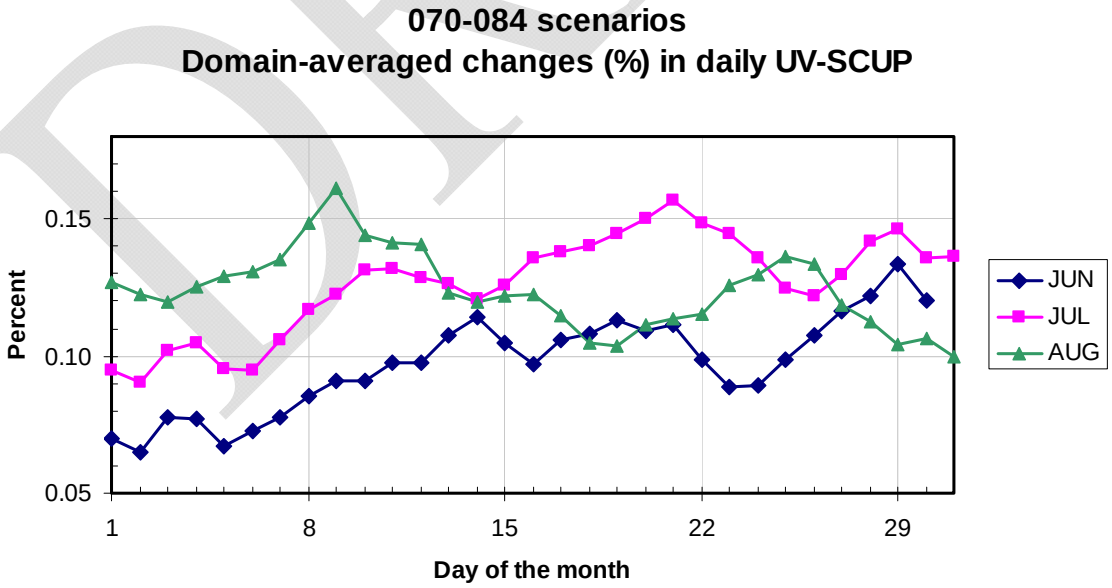

Figure 5: Frequency distribution of percent changes in erythemal surface UV radiation

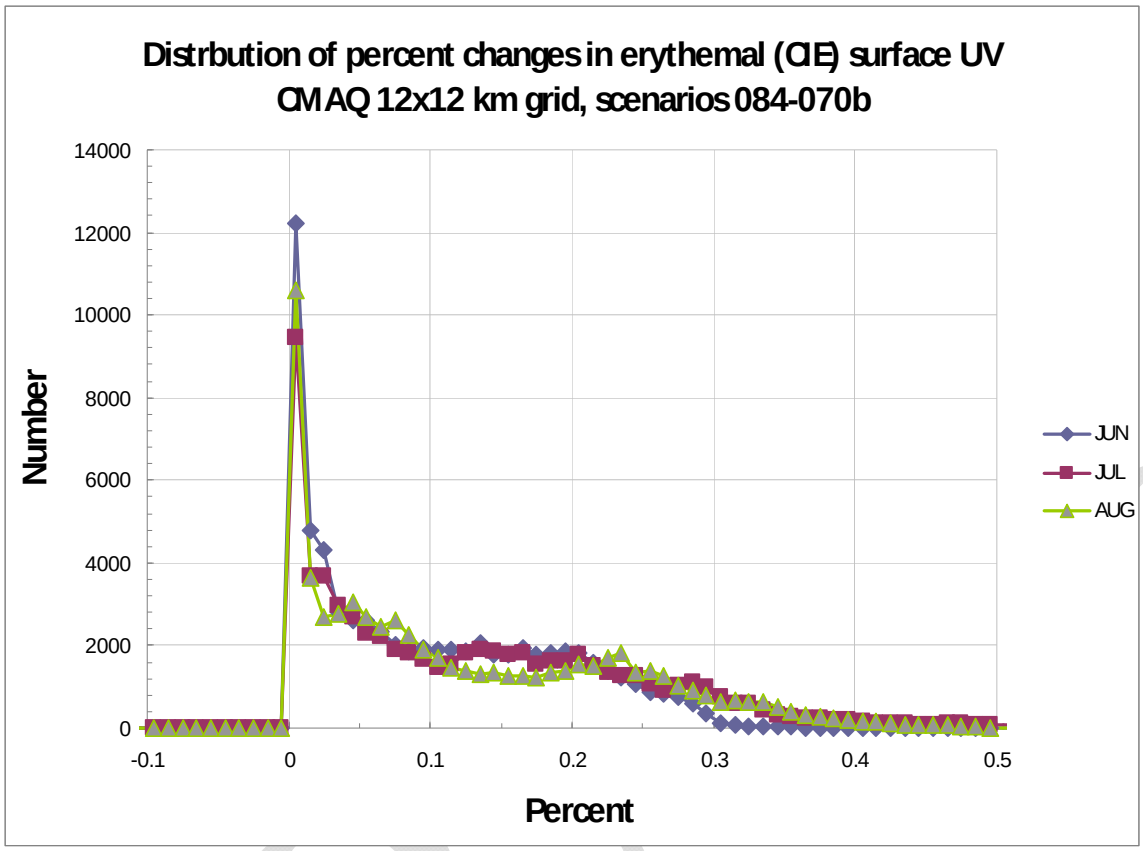

1.3. Population Adjustments

This analysis required county-based population projections for two purposes: to calculate the population-weighted changes in ground level UV for each latitude band modeled in the AHEF model for the year 2020 and to provide future population projections for the years 2005–2050. Although the U.S. Census Bureau provides population projections, they could not be used for this purpose because the publicly available datasets lack the level of detail needed by the AHEF model: population by county, race, gender, and five-year age cohorts. Existing population projections traditionally used by the AHEF model also could not be used because they cover the entire United States, while the area analyzed by CMAQ model covers all or part of 42 states. To meet the data needs of this analysis, county-based population projections were developed using a simple cohort-component methodology.

1.3.1. Cohort-Component Methodology Overview

The cohort-component methodology is a common technique for projecting population changes over time. In this case, three independent components of population change were used: fertility, mortality, and net international migration (i.e., migrations between U.S. counties and foreign countries). Domestic migration (i.e., migrations between U.S. counties) was not included in this projection exercise for reasons discussed below. To project population changes over time, the

population was divided into cohorts that were age-, gender-, and race-specific. Changes due to these three components of change were estimated over time as each cohort was tracked separately, hence the term "cohort-component."

The population of a county in any year *t* as estimated by the model is determined using the following equation:

$$P_t = P_{t-1} + B_t - D_t + NIM_t$$

Equation 1

where:

P_t = Population in year *t*
P_{t-1} = Population in the previous year
B_t = Births in year *t*
D_t = Deaths in year *t*
NIM_t = Net International Migration in year *t*

Beginning with an initial set of populations, annual components of change were applied in the following process, which were repeated annually until the desired end year was reached:

1. Add births by cohort
2. Deduct deaths by cohort
3. Add net international migration
4. Age population one year and repeat for the next year

This methodology is illustrated in Figure 6 below. The cycle begins with an initial Year 2000 population and is repeated until reaching Year 2100.

Figure 6: Demographic model flow

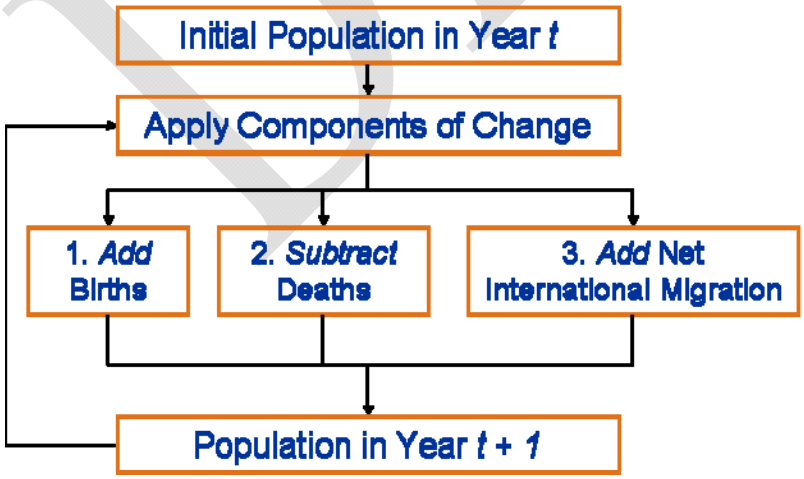

In the following sections, the methods and data used for the initial population and each component are discussed in greater detail.

1.3.2. Component Data and Methods

Initial Population

In order to use the rates for components of change provided by the U.S. Census Bureau (discussed below), it was necessary to begin with an initial Year 2005 population dataset that was disaggregated using the same cohorts. These cohorts in the rates data are divided into two genders (male and female), 100 age groups (0–99 in one year increments), and four racial groups (White, Black, American Indian or Alaskan Native, and Asian or Pacific Islander). This represents 800 distinct population cohorts (2 genders × 100 ages × 4 bridged race groups). County populations using bridged race and one-year age cohorts were most readily accessible using the Vintage 2006 July 1, 2005 dataset provided by the National Center for Health Statistics (NCHS; 2007).

Fertility and Mortality

For fertility, the number of children born equals the number of women in a given cohort times the average number of children born annually to every 1000 women in that cohort divided by 1000. Because virtually all births occur to women between the ages of 10 and 49, only those cohorts were considered in this model. These births are summed by race and used to create a new age zero cohort. To allocate births between males and females, a historic ratio of 1046 males born for every 1000 females born was calculated and it was assumed that this ratio holds steady. Data from the CDC's "Trend Analysis the Sex Ratio at Birth in the United States" were used to complete this calculation (Matthews and Hamilton 2005).
Similarly, mortality was estimated by multiplying the number of people in a given cohort by the cohort-specific mortality rates. The resulting number of deaths was then subtracted from the cohort. Unlike fertility, all cohorts are subject to mortality. Therefore, mortality rates were applied to each cohort. Although an increasing number of Americans are living to the age of 100 or more, the model assumes 100% mortality after age 99 for the sake of computational efficiency. Even with continued rates of survivorship past this age, the 100-plus age group will remain a miniscule portion of the population (0.02% of national population on July 1, 2005).

For fertility and mortality rates, the U.S. Census Bureau's "Component Assumptions of the Resident Population by Age, Sex, Race, and Hispanic Origin" were used (U.S. Census Bureau 2000). These are the same data used in Census projections. These components of change are associated with the 1990 National Projections and were used in both the 1990 State Projections and the 2000 National Projections. While it would be preferable to use more recent data, at this time components of change based on the 2000 Census have not yet been released.

For both fertility and mortality, the so-called Middle Series of component information was used. Fertility rates were provided in a single file; mortality rates for each component were provided in three different tables, for the years 1999–2010, 2015–2055, and 2060–2100. Projected fertility rates were provided for each year to 2100, but beginning with 2010, mortality rates were

provided in five year increments only. We assumed that 2010 mortality rates held steady from 2010–2014, 2015 mortality rates held steady from 2015–2019, and so on.

Net International Migration

The projections for net international migration utilized a simple method based on the Census Bureau's international migration projections for the entire country. These files contain the projected net international migration for each gender, age, and race cohort for the years 2000–2100. Like the fertility and morality rates, these data are part of the Census Bureau's "Component Assumptions of the Resident Population by Age, Sex, Race, and Hispanic Origin" (U.S. Census Bureau 2000). Since the tables "Foreign-born Net Migration to the United States" contain only national level data, it was necessary to allocate the national migrants to the counties. Using 2000 Census data (Summary File 3, Table P22), we determined each county's share of the total population of recent immigrants (i.e., those who entered within the last five years). These county shares were then used to allocate each cohort of immigrants among the nation's counties. The estimated number of immigrants in each cohort was then added to the existing county population of each cohort. This method assumes a constant distribution of recent immigrants based on Year 2000 immigration patterns. While it is likely that new settlement patterns for immigrants will develop in the future, this is the same method the Census Bureau uses for assigning immigrants to states in its state projections (U.S. Census Bureau 2005). The Census Bureau provides a low, medium, and high series for net international immigration. In the base case, the middle series was used.

Domestic Migration

Although domestic migration is also a major component of local population change, it could not be accurately modeled here. The Census Bureau's methodology for state estimates does contain data about state-to-state migration rates based on the observed trend from 1975–2000, but that method does not consider county-to-county migration patterns. The commonly used Woods and Poole projections do consider domestic migration, but are only available to 2030. Developing a method for estimating future migrations was beyond the requirements of this analysis, and likely to introduce more error. The potential impacts of excluding domestic migration from this analysis are discussed in the Section 4.4 which addresses uncertainty in the population adjustments.

1.3.3. Use of these Projections

The population projections developed using the above methodology were used for two purposes in this analysis. First, they were used to calculate the population-weighted change in UV exposure based on the CMAQ and TUV modeling discussed above. These models provided the percent change in ground-level UV exposure for each 12 × 12 km cell in a grid that roughly covers the eastern two-thirds of the United States. To link the change in UV exposure to the population in each county, the average percent change in UV exposure was calculated for each county. In calculating the average for any given county, each cell was given a weighting equal to the percentage of its area of that is located in that county. These county averages were then used to calculate the population-weighted average change in UV exposure for each sex, age group, and latitude band. The modeled population for 2020 was aggregated into male and female, 18 age cohorts (0–4 years, 5–9 years, 10–14 years, and…85-plus years), and three

latitude bands (20–30°, 30–40°, and 40–50°), or 108 population groups (2 sexes × 18 age groups × 3 latitude bands = 108 population groups). For each population group, the population-weighted average exposure was calculated by summing the product of the population in each county multiplied by the change in UV exposure in each county divided by the total population of that population group across all counties.

These projections were also used in the AHEF model runs. Model outputs for each five-year increment from 2005 to 2050 were aggregated for the 108 population groups. Because the CMAQ model did not cover the entire United States, those counties that were not included in the CMAQ modeling area were not included in the aggregated populations.

1.4. AHEF Modeling

The projections of population-weighted percentage change in UV exposure and future populations, as described in Section 2.3.3 above, were inputted into the AHEF model to estimate associated changes in health effects—specifically basal cell carcinoma (BCC), squamous cell carcinoma (SCC), and cutaneous malignant melanoma (CMM) incidences and mortalities.

1.4.1. Overview of Methodology to Estimate Changes in Health Effects

To yield health effects estimates, the AHEF first projected future baseline skin cancer incidence and mortality; this calculation was based on the future population estimates derived in Section 2.3 and baseline incidence and mortality rates for each health effect (based on a scenario of compliance with the Montreal Adjustments to the Montreal Protocol). Then the AHEF multiplied the population-weighted percentage changes in UV exposure in a future year by the appropriate dose-response relationship (described in Section 4.2.2 below) to yield the percentage change in future skin cancer incidence/mortality attributable to the proposed change in the NAAQS ozone standard (from 84 ppb to 70 ppb). These percentages were then multiplied by the baseline incidence and/or mortality for that health effect to compute the absolute number of additional future cases or deaths attributable to the tropospheric ozone standard change.[4] These calculations are shown in Equation 2 below using BCC as an example health effect.

(Cumulative Percentage Increase in UV Exposure) × (Biological Amplification Factor for BCC) × (Baseline Incidence of BCC for the Population Group) = Absolute Increase in BCC Incidence

Equation 2

These calculations were performed for each health effect and for each future population group[5] to produce predictions of the incremental health effects in each future year through 2100 associated with a one-pulse change in the NAAQS ozone standard from 84 ppb to 70 ppb in

[4] This method of multiplying the changes in UV exposure by the biological amplification factor (BAF) and the underlying baseline incidence or mortality is the same as that used by other researchers to estimate changes in health effects based on changes in ozone concentrations (e.g., Madronich and de Gruijl 1994, Pitcher and Longstreth 1991).
[5] The future population group is a subset of the total U.S. population, calculated specifically for this analysis, as described in Section **Error! Reference source not found.** above.

2020. It is important to note that because the percentage increase in UV exposure associated with the tightening of the NAAQS standard from 84 ppb to 70 ppb is being used as the environmental input in the AHEF, only the incremental number of health effects associated with the standard change were modeled. The absolute number of health effects associated with the current NAAQS standard was not expressly calculated.

1.4.2. Selected Action Spectrum and Derived Dose-Response Relationships

The calculation of incremental health effects in Equation 2 above involves the use of a derived dose-response relationship, or biological amplification factor (BAF). Determining the health effects caused by UV exposure first requires information on the relative weights to be placed on each discrete UV wavelength to reflect the degree to which each wavelength causes biologic damage. Such a weighting function is called an action spectrum—an experimentally derived function that describes the relative effectiveness of each UV wavelength in the induction of skin cancers. The AHEF relies on action spectra for each health effect because action spectra provide information regarding which wavelengths of the total UV spectrum are most effective at causing the particular health effect. Based on the available action spectra, the Skin Cancer Utrecht-Philadelphia-human (SCUP-h) action spectrum (derived based on the induction of SCC in hairless mice and corrected for human skin transmission) was selected for modeling SCC, BCC, and CMM in the AHEF.[6]

Based on the action spectrum selected for each health effect, the relationship between those health effects and the intensity of UV exposure can then be explored. These dose-response relationships are derived by correlating measurements or estimates of UV exposure received for a specific action spectrum and given health effect at various locations, and the level of incidence or mortality for that health effect at those same locations. In the AHEF, statistical regression analyses were used to estimate the dose-response relationship, known in technical terms as the BAF, for each health effect. The BAF measures the degree to which changes in UV exposure weighted by the appropriate action spectrum (as measured in Watts/m^2) cause incremental changes in health effects (incidence or mortality), and is estimated after accounting for the influence of birth year and age, as necessary.

BAFs are defined as the percent change in a health effect resulting from a one-percent change in the intensity of UV radiation (weighted by the chosen action spectrum). For example, for BCC incidence in white males, a one-percent change in the intensity of UV radiation results in a 1.5 percent change in BCC incidence. For each health effect, the AHEF applies the BAF to predict future incidence and mortality as shown in Equation 2 above.

Table 3 presents a summary of calculated BAFs and selected action spectra for each health effect.

[6] Since a mammalian action spectrum for CMM still remains to be determined, the SCUP-h is also used to model CMM.

Table 3: Summary of Calculated BAFs, Selected Action Spectra, and Key Inputs

Health Effect	Data Sources	Selected Action Spectrum	BAF: Used in AHEF (Annual Exposures)	
			Males	Females
CMM Incidence/ Mortality	*Incidence*: Ratios from SEER data set *Mortality*: EPA/NCI data set *BAF*: Developed using econometric analysis	SCUP-h (1993)	0.5846	0.5047
BCC Incidence	*Incidence:* Based on methods used in U.S. EPA (1987) and Fears and Scotto (1983) *BAF:* de Gruijl and Forbes (1995)	SCUP-h (1993)	1.5	1.3
SCC Incidence	*Incidence:* Based on methods used in U.S. EPA (1987) and Fears and Scotto (1983) *BAF:* de Gruijl and Forbes (1995)	SCUP-h (1993)	2.6	2.6
Nonmelanoma Mortality	*Mortality:* EPA/NCI data set *BAF*: Developed using econometric analysis	SCUP-h (1993)	0.7094	0.4574

1.5. Valuation of Human Health Effects

The monetary value of incremental cases of basal cell carcinoma (BCC), squamous cell carcinoma (SCC), and cutaneous malignant melanoma (CMM) was calculated as the number of additional cases multiplied by the medical and productivity loss cost per case. Cost per case is for cancer care only and excludes the costs of unrelated care, such as increased costs for treating other medical conditions later in life that might have occurred after the projected skin cancer mortality. For a change in the NAAQS ozone standard in one year (2020) only, the AHEF output gave the associated increase in skin cancer incidence and mortality, by health effect type, in each year through 2150. Total incremental costs were calculated over 2020–2150 and discounted to 2020 using discount rates of 3 percent and 7 percent, consistent with the guidance provided in the Office of Management and Budget's (OMB) (2003) Circular A-4.

The medical costs and productivity loss per case are shown in Table 4. These monetary values (in 2005$) were employed in a peer-reviewed publication (Kyle et al. forthcoming).

Table 4: Total Cost per Case of Non-fatal Skin Cancer and Mortality (2005 $)

		Medical Cost	Productivity Loss Cost	Total Cost per Case/Mortality
Non-fatal Skin Cancer Case				
	Basal Cell Carcinoma	$1,066*	$1,161†	$2,228
	Squamous Cell Carcinoma	$1,066*	$4,477†	$5,543
	Cutaneous Malignant Melanoma	--	--	$37,220‡
Skin Cancer Mortality				$6.6 million§

* Chen et al. (2001), adjusted to 2005 $ using the medical care component of the Consumer Price Index (CPI-U).

† Calculated by ICF, based on U.S. EPA (1988) and U.S. BLS (2007).
‡ U.S. EPA (1988), adjusted to 2005 $ using the CPI-U for medical care.
§ Adjusted from $5.5 million at 1990 income levels (2000 $) to $6,600,000 at 2020 income levels. $5.5 million is the mean of a normal distribution with a 95% confidence interval between $1 million (Mrozek and Taylor 2002) and $10 million (Viscusi and Aldy 2003).

Medical costs per case of BCC and SCC were based on Chen et al. (2001); this study used data from the Medicare Current Beneficiary Survey (1999–2000) to estimate medical treatment costs associated with BCC and SCC in different practice settings. To determine an average medical treatment cost per case, weighted averages were calculated based on the percentage of episodes managed in each setting.

Productivity loss costs were based on a U.S. EPA analysis supporting the Regulatory Impact Analysis: Protection of Stratospheric Ozone (U.S. EPA 1988). The cost per case was calculated by multiplying EPA's estimates of the loss of work due to illness and care giving performed by others for the patient for BCC and SCC by the national mean annual wage for 2005 (U.S. BLS 2007). For CMM, EPA's estimate of the total medical cost and productivity loss per case was used and adjusted to 2005 $ using the CPI-U for medical care (U.S. EPA 1988).

The value of a statistical life (VSL) is estimated to be $5.5 million at 1990 income levels and $6.6 million at 2020 income levels. The estimate of $5.5 million is the mean of a normal distribution with a 95 % confidence interval between $1 and $10 million. The confidence interval is based on two meta-analyses of the wage-risk VSL literature: $1 million represents the lower end of the interquartile range from the Mrozek and Taylor (2002) meta-analysis; and $10 million represents the upper end of the interquartile range from the Viscusi and Aldy (2003) meta-analysis. The VSL represents the value of a small change in mortality risk aggregated over the affected population.

Results

This section provides an overview of the results of this analysis, including changes in ground level SCUP-h UV, changes in health effects (i.e., incremental skin cancer incidence and mortalities), and the resulting monetized disbenefits.

1.6. Changes in Ground Level SCUP-h UV

Using the methodology described in Section 2 above, the percent change in ground-level SCUP-h UV was calculated for each day and averaged across each month. The figures below represent average changes in SCUP-h UV associated with achieving an ozone standard of 70 ppb (down from 84 ppb) in the summer months of June, July, and August.

Figure 7: Ground Level UV Percent Change between 70 and 84 ppb, June

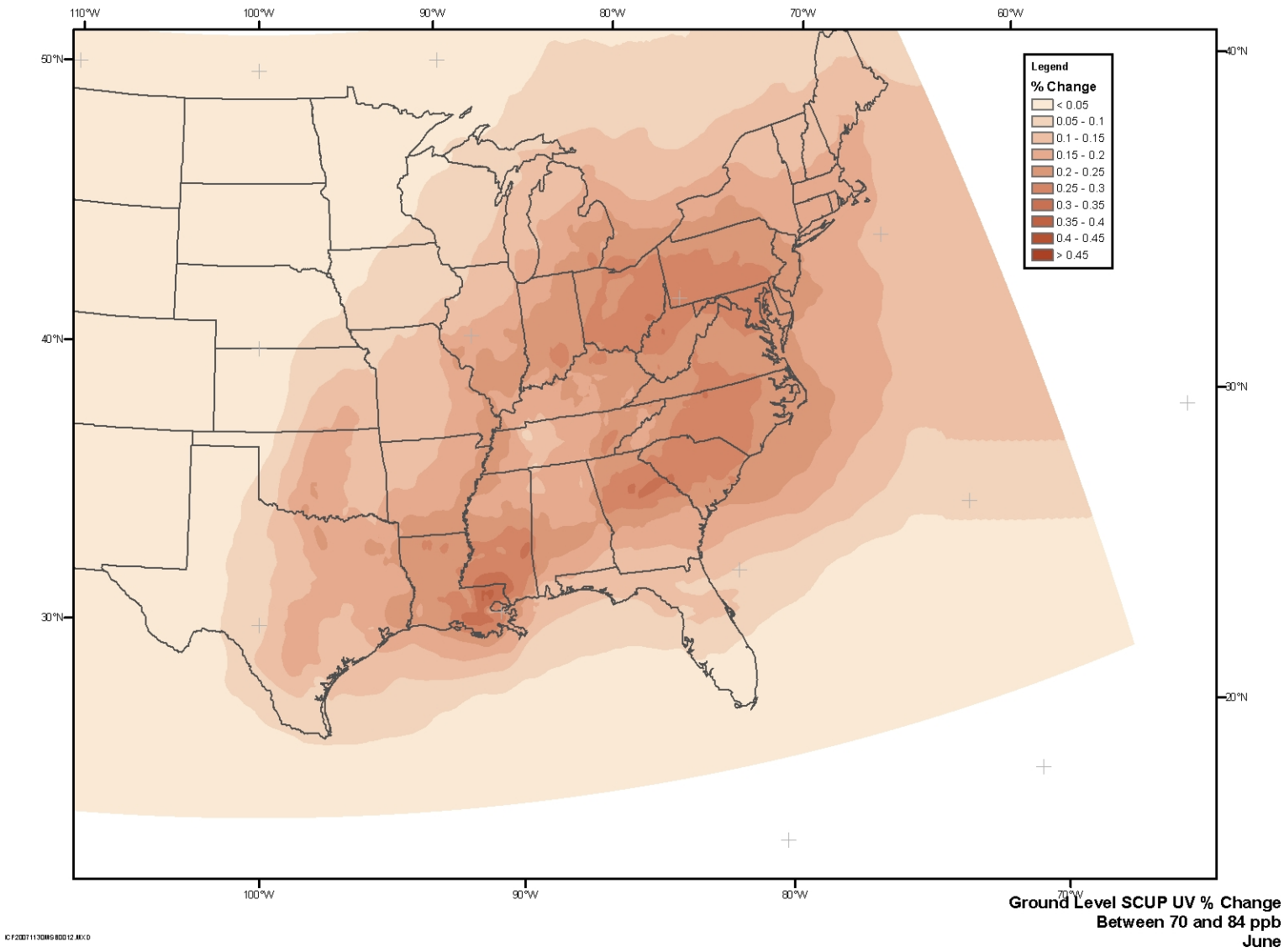

Figure 8: Ground Level SCUP-h UV Percent Change between 70 and 84 ppb, July

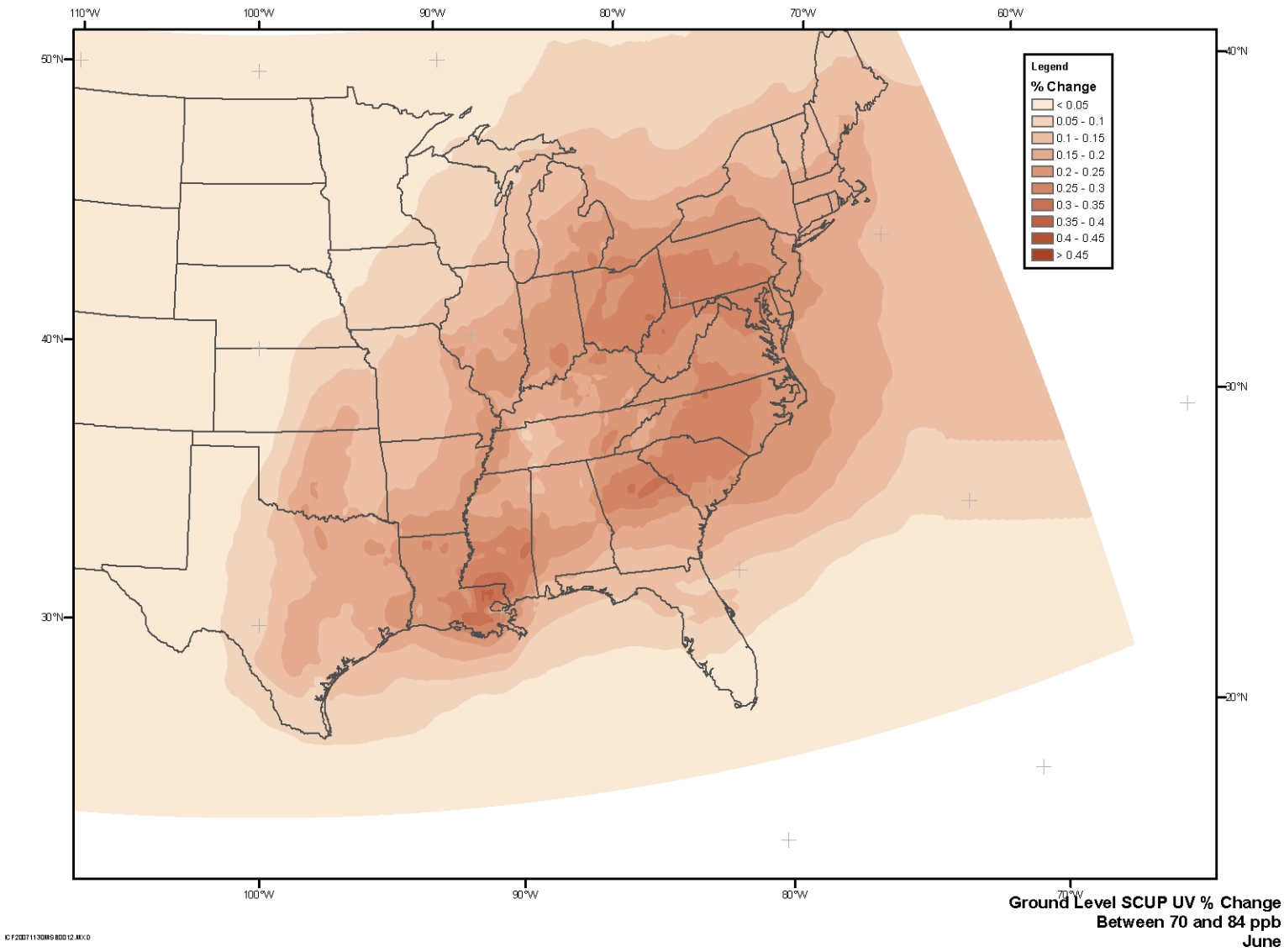

Figure 9: Ground Level SCUP-h UV Percent Change between 70 and 84 ppb, August

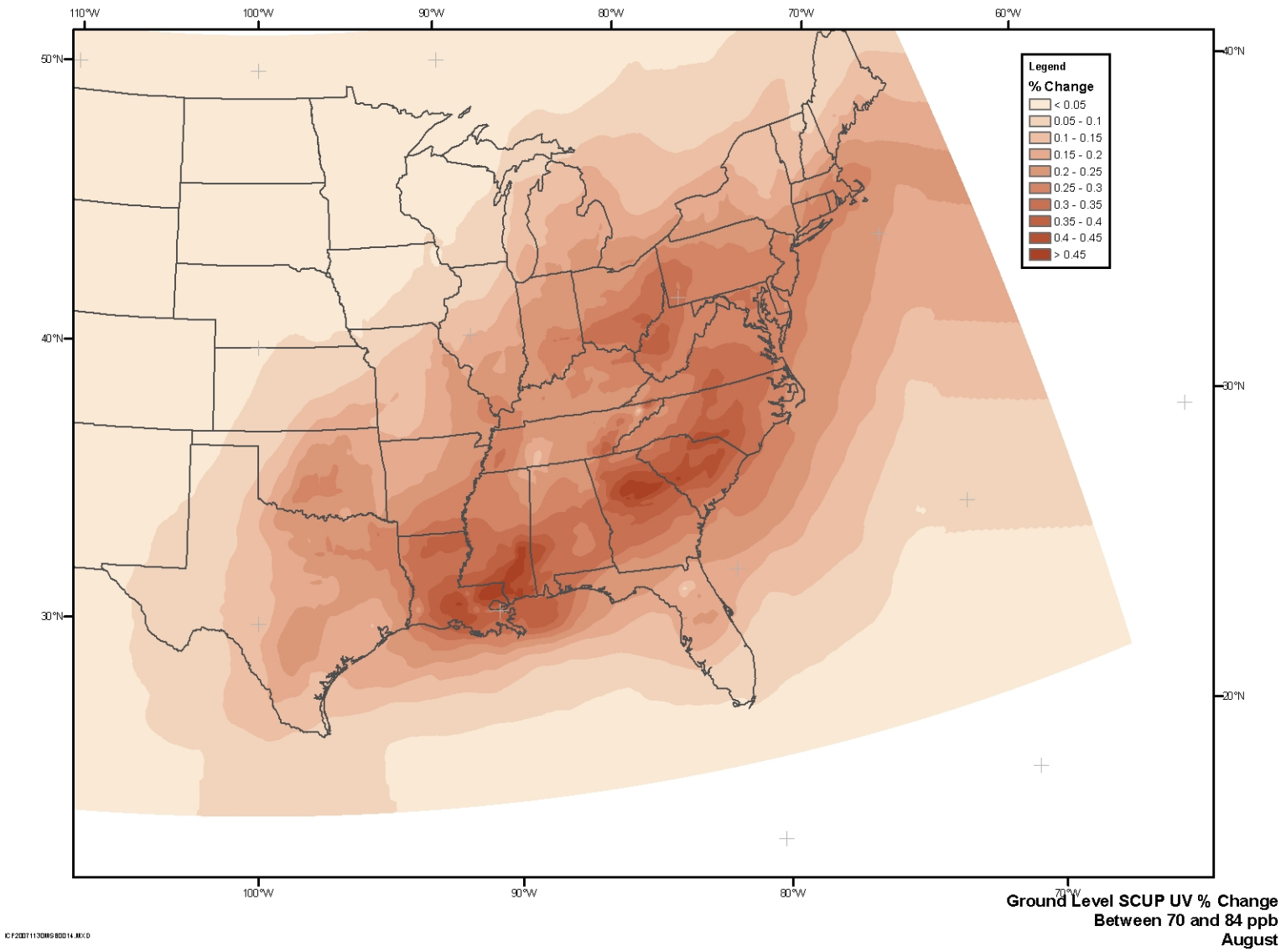

1.7. Changes in Human Health Effects

This section presents results in terms of the changes in skin cancer incidence and mortality associated with a one-year change in the ozone standard in 2020. Table 5 below gives the cumulative change in incidence and premature mortality associated with a one-time pulse (i.e., a change in the ozone standard from 84 ppb to 70 ppb in one year, 2020). As shown, 3,538 additional cases of skin cancer and about 16 additional mortalities are expected. For the age cohorts relevant to this analysis (those populations potentially alive in 2020 and thereafter; i.e., those born from 1930 to 2100) and for the population subset analyzed, baseline skin cancer modeled in the AHEF through 2150 totals more than 188 million cases and about 2.6 million mortalities. Thus, the additional cases and mortalities associated with changing the ozone standard represent less than 0.002% and less than 0.001% of baseline, respectively.

This section also provides the monetary value of those future health effects, discounted back to 2020, in Table 6 and Table 7.

Table 5: Additional Skin Cancer Incidence and Mortality Associated with a Change in the Ozone Standard in 2020

Skin Cancer Type	Incidence	Mortality
	Central Estimate* *(Uncertainty Range†)*	
Nonmelanoma Skin Cancer	3,454 *(2,348–4,560)*	5.7 *(3.9–7.5)*
Cutaneous Malignant Melanoma	84 *(57–110)*	10.5 *(7.1–13.8)*
Total	3,538 *(2,405–4,671)*	16.2 *(11.0–21.3)*

* From the AHEF model.
† The uncertainty range is derived by applying the quantified uncertainty (approximately 32%), as calculated in Section 1.15, to the central estimate.

Table 6: Monetized Summary Table (3% discount rate, discounted to 2020 with prices in 2005 $)

Skin Cancer Type	Incidence	Mortality
	Central Estimate* *(Uncertainty Range†)*	
Nonmelanoma Skin Cancer	$4,717,452 *($3,207,130–$6,227,773)*	$13,334,430 *($9,065,329–$17,603,530)*
Cutaneous Malignant Melanoma	$1,399,631 *($951,531–$1,847,732)*	$28,630,454 *($19,464,236–$37,796,672)*
Total	$6,117,083 *($4,158,661–$8,075,505)*	$41,964,884 *($28,529,566–$55,400,202)*

* Based on incidence and mortality projected by the AHEF model.
† The uncertainty range is derived by applying the quantified uncertainty (approximately 32%), as calculated in Section 1.15, to the central estimate.

Table 7: Monetized Summary Table (7% discount rate, discounted to 2020 with prices in 2005 $)

Skin Cancer Type	Incidence	Mortality
	Central Estimate* *(Uncertainty Range†)*	
Nonmelanoma Skin Cancer	$2,234,469 *($1,519,090–$2,949,848)*	$5,819,781 *($3,956,542–$7,683,021)*
Cutaneous Malignant Melanoma	$720,816 *($490,042–$951,590)*	$14,068,218 *($9,564,191–$18,572,246)*
Total	$2,955,285 *($2,009,132–$3,901,438)*	$19,888,000 *($13,520,733–$26,255,267)*

* Based on incidence and mortality projected by the AHEF model..
† The uncertainty range is derived by applying the quantified uncertainty (approximately 32%), as calculated in Section 1.15, to the central estimate.

Uncertainty

1.8. Uncertainty in estimated impacts

Uncertainty in the estimation of human health impacts arising from a tightening of the NAAQS standards from 84 ppb to 70 ppb arise from various sources. These uncertainties are addressed in the following sections:

- **CMAQ Modeling**—uncertainty in the prediction of precise tropospheric ozone column changes under the NAAQS scenarios
- **TUV Modeling**—uncertainty in the calculation of consequent changes in surface UV-SCUP
- **Population Adjustments**—uncertainty in the determination of county based population projections
- **AHEF Modeling**—uncertainty in the estimate of associated changes in health effects including latency
- **Valuation Of Human Health Effects**—uncertainty in the monetary value of incremental skin cancer incidence/mortality
- **Unquantified Sources of Uncertainty**—other qualitative sources of uncertainty
- **Summary of Quantified and Unquantified Sources of Uncertainty**

The sources and magnitudes of the uncertainties associated with each step of the analysis were identified and are discussed in the relevant sections below.

1.9. Uncertainty in CMAQ Modeling

Output from CMAQ modeling runs from U.S. EPA (CMAQ version 4.5) were provided for the two NAAQS scenarios with identifiers:

- 2020bk_v4.5_084_12km.o3_hr_shift_LST, and
- 2020bk_v4.5_070b_12km.o3_hr_shift_LST

The CMAQ model did not cover the entire United States, the area analyzed covers all or part of 42 states in the eastern two-thirds of the country

Eder and Yu (2006) have conducted performance evaluations comparing annual simulations (2001) of CMAQ (version 4.4) covering the contiguous United States against monitoring data for four nationwide networks. This effort represents one of the most spatially and temporally comprehensive performance evaluations of the model. Simulations of the peak 1- and 8-h ozone concentrations during the summer (April–September) were "relatively good" (correlation (r)=0.68, 0.69; normalized mean bias = 4.0 %, 8.1 % and normalized mean error = 18.3 % and 19.6 % respectively). No performance evaluation could be assessed for the provided scenarios; however, analysis for the CMAQ review process (see http://www.cmascenter.org/index.cfm) typically returns normalized mean errors for ozone ≈ 20%.

As described in Section 2.2, the CMAQ ozone concentrations are accommodated into the TUV model to determine overall column ozone values.

1.10. Uncertainty in TUV Modeling

1.10.1. Uncertainty Analysis of TUV Calculations

The uncertainties in the TUV calculations can be divided into two types:

1) Uncertainties inherent in the TUV numerical model, primarily from the approximate 2-stream (delta-Eddington) solution of the radiative transfer equation, and the discretization of altitudes and wavelength and related interpolations. These uncertainties have been shown in many earlier studies to be negligible, on the order of 5% or less, when compared to higher stream models and higher vertical and spectral resolution.

2) Uncertainties in the input parameters that describe atmospheric composition (vertical profiles of air, ozone, other absorbing gases, aerosols, and clouds) and the earth's surface reflectivity.

If the input parameters are well known (e.g., cloud-free and pollution-free conditions with measured total ozone column as inputs), the TUV results are accurate to a few percent, which is also the accuracy of the best instruments for measuring atmospheric UV radiation. For the present purposes, the inherent TUV uncertainty (item 1) is taken, conservatively, as 5%.

The atmospheric input parameters (item 2 above) are generally not well known in any specific situation, and are highly variable spatially and temporally, with long-term trends also a possibility. For the purposes of these calculations, we adopt the principle that UV changes

stemming from CMAQ scenario changes in tropospheric ozone can be calculated under the premise that **all other atmospheric conditions remain exactly the same between the two scenarios**, including clouds, aerosols, and surface reflectivity. This is consistent with the approach used in calculations relating stratospheric ozone changes to surface UV increases.

Table 8 shows the predicted changes in UV-SCUP calculated by the TUV model, between the two CMAQ scenarios (084 to 070), for 15 July. The changes are expressed as percent changes in daily UV-SCUP doses at each location, then domain-averaged to give the values in the third column of the table. The reference model (test number 0) would be used in the AHEF estimates of skin cancer changes. The other entries in the table (tests number 1–6), show the UV-SCUP % change between scenarios, if other atmospheric conditions are changed individually and equally for both scenarios, as described in the second column. The last column gives the % effect of changing the atmospheric conditions. For example, the reference calculation (test 0) gives a UV-SCUP increase of 0.118% in going from scenario 084 to 070. If aerosols are removed from the model (test 1), the UV-SCUP increase between scenarios is only 0.112, which is a 5.1 % reduction relative to the reference case. A brief explanation of the effects from each factor is given below.

Table 8: UV-SCUP changes between CMAQ scenarios 084 and 070 on 15 July, for different values of other factors (aerosol, surface albedo, clouds, and stratospheric ozone).

Test number	Description	Domain-averaged change in UV-SCUP, %	Effect of other factors, %
0	Reference (Elterman* aerosols, 10% surface albedo, no clouds, sea level, USSA stratospheric O_3)	0.118	≡ 0
1	No aerosols	0.112	-5.1
2	0% surface albedo	0.112	-5.1
3	High thin cloud, at 9-10 km, optical depth =2	0.132	11.9
4	Low moderately heavy cloud, at 1-2 km, optical depth = 16	0.169	43
5	850 mb surface pressure	0.098	-17
6	20 DU reduction in stratospheric O_3 (above 16 km)	0.123	4.2

(*) Elterman continental aerosol vertical profile, with total optical depth (at 550 nm) = 0.235, Angstrom alpha = 1.0, single scattering albedo = 0.99, asymmetry factor = 0.61.

1. Aerosols increase the photons' pathlengths, and therefore increase the probability of absorption by tropospheric ozone. By removing aerosols from the reference run, the UV increase from changing ozone scenarios is somewhat smaller.

2. Surface albedo reflects light back to the atmosphere, and a fraction of this can be scattered back toward the surface, effectively increasing the photons' path-lengths for absorption by tropospheric ozone. If the surface is not reflecting (albedo = 0%), these photon reflections do not occur and the interaction with tropospheric ozone is smaller.

3. High clouds (e.g., cirrus) make the incident (down-welling) light more diffuse and therefore more slanted as it passes the troposphere. They also reflect a fraction of the up-welling radiation (up-scattered by tropospheric molecules), back to the lower troposphere (much like surface albedo, but in the opposite direction). Both effects increase tropospheric photon pathlengths and therefore the probability of absorption from any additional tropospheric ozone.

4. Low thick clouds (e.g., stratocumulus, marine stratus) have a larger effect because they are at altitudes closer to where the ozone changes are largest. In-cloud increases of ozone are particularly significant because of the long in-cloud photon pathlengths, as has been observed and modeled (e.g., Mayer et al., 1997). Broken clouds (e.g., fair-weather cumulus) are expected to be intermediate between fully overcast and fully clear (Nack and Green, 1974).

5. Decreases in atmospheric pressure reduce, in direct proportion according to the ideal gas law, the conversion factor between ozone molar mixing ratios (ppb, specified by CMAQ) and the ozone number density (molecules cm^{-3}, which is integrated to obtain the ozone column in Dobson Units) used for atmospheric transmission. Also, lower pressures decrease the Rayleigh optical depth and therefore the photon path coupling between scattering and absorption. These factors combine to yield a smaller SCUP-UV change. The pressure reduction chosen here, 850 mb, is roughly representative of cities at high elevation. Thus, this case can also be considered a surrogate test for the effect of surface elevation (varying the surface elevation directly is possible within the TUV code, but would have created some ambiguity between the nominal CMAQ altitudes and the TUV geometric grid).

6. Reductions in stratospheric ozone imply that any tropospheric ozone changes are a larger fraction of the total column ozone. Therefore the sensitivity to CMAQ scenario changes is greater if the stratospheric ozone is smaller. This is consistent with the power law first proposed by Madronich (1993):

$$UV_{\text{bio}} \propto (DU)^{-RAF}$$

for which the theoretical basis is described by Micheletti et al. (2003).

The sensitivity studies (cases 1-6) show that how the baseline environmental conditions, under which the difference between the two tropospheric ozone scenarios was assessed, could contribute to the uncertainties of the TUV-calculated changes in surface SCUP-UV radiation. The worst case is that of low clouds: If the entire domain were actually covered by low clouds for the entire period of interest (June–August), the TUV calculations made under cloud-free assumption would underestimate the UV increases stemming from the changes in tropospheric ozone, by about 43%. This extreme case is patently unrealistic. Conservatively, if it is assumed

that low clouds are present no more than 1/4 of the time, their error is reduced to about 11%. Thus, the uncertainty budget can be summarized as follows:

Inherent TUV uncertainties	5	%
Aerosols	5.1	%
Surface albedo	5.1	%
High clouds	11.9	%
Low clouds (1/4 of the time)	11	%
Surface pressure	17	%
Stratospheric ozone	4.2	%
TOTAL (quadrature)	25	%

For example, for the 15 July case, the reference UV-SCUP change of 0.118 % is estimated to be, with high certainty, in the range 0.088–0.148 %.

Finally, it should be noted that these estimates are generally overly conservative. For example, high clouds are likely to be present only a fraction of the time, and the 850 mb pressure may apply to only a few locations. Therefore the 25% uncertainty estimated here should be viewed as a very conservative upper limit.

The TUV model also has the option of calculating radiation incidence on a sphere or on a horizontal plane. Incidence on a sphere is presently considered a better metric for UV exposure and was therefore used in this analysis. A small uncertainty is introduced over incidence on a horizontal plane, the previous standard. The percent change in UV is reduced by about 8 % by taking the spherical output in preference to the planar output (i.e., for the 15 July domain-average, from 0.126 % to 0.118 %). This is a small effect and it should be noted that the average SCUP-UV changes are still near 0.1 % using either output.

1.10.2. Comparison with UV Changes Due to Other Factors

In Section 2.2.3, the UV-SCUP change resulting from tropospheric ozone change between the two CMAQ scenarios was calculated and shown to be of order ~ 0.1 %, if all other environmental factors are kept constant between the two scenarios. Below, we consider, for comparison only, the UV changes that would result if these other factors are allowed to vary between two scenarios. To illustrate this, Table 9 shows the UV changes, calculated for the CMAQ 084 tropospheric ozone scenario, when other environmental conditions, rather than tropospheric ozone, are changed relative to the reference conditions. The magnitude of changes in the conditions is the same as used for Table 8. **It should be emphasized that the % UV changes shown in Table 9 are NOT those associated with changes in tropospheric ozone, but rather with direct changes in the other environmental conditions.**

Table 9: Effect on surface SCUP-UV radiation of varying environmental conditions other than tropospheric O_3.

Test number	Description	Domain-averaged % change in UV-SCUP
0	Reference (Elterman aerosols, 10% surface albedo, no clouds, sea level, USSA stratospheric O_3), tropospheric O_3 scenario 084	≡ 0
1a	No aerosols	7.3
2a	0% surface albedo	-3.8
3a	High thin cloud, at 9-10 km, optical depth =2	-12.1
4a	Low moderately heavy cloud, at 1-2 km, optical depth = 16	-50.
5a	850 mb surface pressure	10.4
6a	20 DU reduction in stratospheric O_3 (above 16 km)	7.6

Should the baseline environmental conditions actually change **between** the two CMAQ tropospheric ozone scenarios (084 and 070), the SCUP-UV changes could be far larger. Of course, there is no solid scientific basis for expecting such environmental changes in response to relatively small changes in tropospheric ozone. Some interactions are known, (e.g. oxidant photochemistry leading to the formation of sulfate and secondary organic aerosols, which can affect radiation directly as well as change cloud nucleation and lifetimes) but these effects are still poorly quantified, and although subjects of active current research, are not expected to be as large as the variations used in this sensitivity analysis.

1.11. Uncertainty in Population Adjustments

The Cohort-Component Methodology (see Section 2.3.1) for population adjustment used in the analysis gave a 2020 total population of 336.1 million in very close agreement with the U.S. Census Bureau projection for 2020 of 335.8 million—a difference of less than 0.1 %. However, as discussed above, the model did not consider domestic migration between counties due to the lack of suitable alternative estimates. It is assumed that migration between neighboring counties within the same metropolitan area is not likely to have an impact on the results because the change in ozone concentration is similar in adjacent areas. When aggregated across broad latitude bands with hundreds of counties, small differences from one county to the next due to migration are likely to cancel each other out.

Interregional migration—such as the observed historic migrations from the Northeast and upper Midwest to the Sun Belt states—is a potential source of uncertainty in this analysis. Since the model estimated that all local populations change only through births, deaths, and the arrival of international immigrants, it is possible that populations of regions that are losing migrants to

other parts of the country are overrepresented in this analysis, while the populations of fast-growing regions attracting these migrants are underrepresented. Because the population-weighted change in UV exposure is higher in the southern latitude band than in the northern latitude band, this analysis may be underestimating the change in exposure if the historic north-to-south migration pattern holds. However, this effect is not uniform—Florida, for example, exhibits much lower changes in UV than other areas of the South, but has traditionally received a large portion of migrants from the North.

Ultimately, it was decided that the uncertainty associated with predicting migration patterns outweighed the uncertainty introduced by excluding domestic migration from this model. Because migration between regions is a matter of percentage points rather than degrees of magnitude, it is assumed that the overall uncertainty associated with the population projections is relatively small.

The CMAQ model area also has population implications. The area analyzed covers all or part of 42 states in the eastern two-thirds of the country. As a result, those counties that were not included in the CMAQ modeling area were not included in the aggregated populations (26.2 % of the total population). It would be reasonable to assume, given this truncation of population (e.g., 13.5 % of the population reside in California) and the historically high proportion of cases of skin cancer and/or mortality on the West Coast (e.g., California counties, especially Los Angeles), that this input alone would introduce a disproportional large, unquantifiable uncertainty if the estimated health effects from the analysis were extrapolated to the rest of the population. Therefore, the results of this analysis must be viewed in this context when drawing comparisons with other studies which consider the continuous United States (e.g., Lutter and Wolz, 1997).

1.12. Uncertainty in AHEF Modeling

AHEF modeling contributes uncertainties to the estimates of human health effects—resulting from a change in NAAQS standards—in two major areas:

1) the dose-response relationships (expressed as a BAF) for the three endpoints of concern (i.e., BCC, SCC, and CMM), and

2) the future size, behavior, and distribution of the populations that will be affected (see Section 4.4. Uncertainty in Population Adjustments).

It should be noted that for this analysis, only estimated uncertainty in the BAF parameter is quantifiable.

1.12.1. Uncertainties in Selected Derived Dose-Response Relationships

The AHEF model (described in Section 2.4) incorporates information on the dose-response relationships for BCC, SCC, and CMM through the use of a BAF (i.e., the slope of the dose-response relationship). . The estimate of BAF and associated standard error generated for CMM incidence/mortality using the SCUP-h action spectrum is 0.5846 ± 0.02 for males, 0.5047 ± 0.02 for females which yields an uncertainty range of approximately 3 % for changes in these health

effects estimates; the BAF and associated standard errors generated for NMSC mortality 0.7094 ± 0.03 for males, 0.4574 ± 0.03 for females which yields an uncertainty range of approximately 4 and 7 % respectively; and BAFs and associated standard errors generated for BCC and SCC are 1.5 ± 0.5 for males, 1.3 ± 0.4 for females and 2.6 ± 0.7 for males, 2.6 ± 0.8, respectively (deGruijl and Forbes, 1995) which yields an uncertainty range of approximately 30% for changes in these health effects estimates.

1.12.2. Behavioral Uncertainties

While the AHEF assumes that human exposure behavior remains constant over time, changes in human behavior affect the amount of UV radiation exposure received. For example, changes in (1) the amount of time spent outdoors, (2) in socioeconomic profiles that impact travel to areas where high UV exposure can be expected (i.e., the beach), or (3) in the use and/or efficacy of sun protection technologies such as sunglasses and sunscreens can impact the extent of UV exposure received.

A number of recent studies have examined UV exposure behaviors in the U.S. Godar et al. (2003) found that Americans get about 23 % of their lifetime UV dose by the age of 18, 46 % by the age of 40, and about 74 % by the age of 59, assuming that individuals live up to the age of 78. Among U.S. youth ages 11–18, Cokinnides et al. (2001) found that about 10 % reported practicing three or more sun protection behaviors regularly and nearly 60 % practiced one or two routinely; however, about one-third of the youth overall did not practice any recommended sun protection behaviors.

1.12.3. Latency

Another source of uncertainty in the AHEF health effects estimate is associated with the exposure period over a person's lifetime that is most likely to be the cause of UV-related health effects. This is especially relevant for CMM, since it has been hypothesized that CMM is largely the product of intense exposures early in life (e.g., through age 20) rather than cumulative lifetime exposure. The AHEF uses whole life exposure for all skin cancer types as the default assumption. Using early life exposure for CMM is not the same as evaluating a latency effect, but can be used as a proxy for latency in this health end point. Figure 10 shows the effect of this proxy measure for latency on CMM mortality changes by ≈ 10 percent when the exposure assumptions (early life *versus* whole life) are changed (U.S. EPA, 2003), with uncertainty concerning the appropriate exposure dose manifesting itself less in the total incremental risks predicted, than in *when* those incremental effects are predicted to occur, and *who* will bear them (i.e., shifting the risk to future generations). Modeling this lag time further is difficult given the current state of knowledge about latency and its mechanisms (Madronich, 1999).

Figure 10: Excess CMM mortality for the Montreal Adjustment scenario for equal-age exposure weighting and weighting for exposures only for ages 1–20: cumulative annual exposure (U.S. EPA/NASA, 2001).

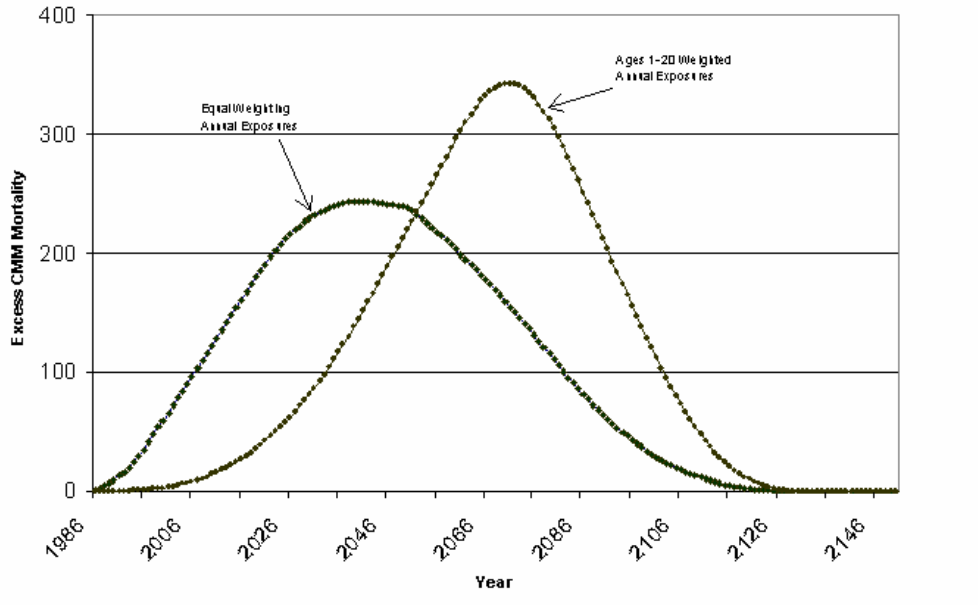

1.13. Uncertainty in Valuation of Human Health Effects

An extensive literature review was conducted to determine the best medical cost estimates for NMSC for the Economic Evaluation of the U.S. Environmental Protection Agency's SunWise Program: Sun Protection Education for Young Children (Kyle et al., forthcoming). Values were taken from Chen et al. (2001), considered to be the best available source of data for these health endpoints; however, the authors did not include uncertainty bands around their central estimates.

The national mean annual wage for 2005 (U.S. BLS, 2007) is $37, 870 (mean annual wage for all occupations) which has a mean relative standard error of 0.1%.

1.14. Unquantified Sources of Uncertainty

There are a number of other sources of uncertainty in the analysis' health effects predictions. Some of these sources of uncertainty are possible to quantify, but are not central to the structure of the analysis. Others cannot be quantified because any assumptions or estimates would be simply speculative. These other sources of uncertainty include:

- Composition of the future atmosphere;
- Future conditions of the ozone column;
- Effect of climate change;
- Compliance with modeled policy scenarios;
- Laboratory techniques and instrumentation for deriving action spectra;
- Improvements in medical care/increased longevity; and
- Baseline information.

These uncertainties are described qualitatively in more detail below.

Composition of the Future Atmosphere

The exact composition of the future atmosphere as a result of compliance with different policies (i.e., ODS phaseout under the Montreal Adjustments to the Montreal Protocol) is unknown. As levels of atmospheric chlorine are reduced, the impact of ozone depletion from chlorine and bromine radical species generated from ODS would change. In addition, long-term systematic changes in atmospheric opacity (e.g., clouds, aerosols, other pollutants) will also impact the ability to model changes in ozone. Likewise, future changes in climate could result in changes in the atmospheric circulation patterns and therefore could change cloud cover. The impacts of such changes on the predicted recovery of the ozone layer and subsequently tropospheric ozone are unknown. All of these uncertainties could influence the ability to model atmospheric processes accurately.

Future Conditions of the Ozone Column

Uncertainties also can be contributed by assumptions regarding the future conditions of the ozone column in response to the phaseout of ODS. Some computer models predict that the phaseout of ODS will slow and eventually stop the rate of ozone depletion, and suggest that natural ozone-making processes will enable stratospheric ozone to return to 1979–1980 ozone conditions. These models also predict that the recovery will eventually result in increased concentrations beyond 1979–1980 levels[7] (see Chapter 12 in WMO 1999 for more detail). Because there is incomplete knowledge about the behavior of ozone prior to the satellite measurements taken in 1979–1980, the AHEF imposes a limit on future ozone recovery to the conditions observed in 1979–1980.

Effect of Climate Change

The effects of global climate variations on stratospheric temperature and, in turn, on ozone depletion, are not well understood, and have therefore not been assessed in the analysis. While this effect is not typically incorporated into models used to assess future ozone depletion, it does represent a modeling constraint that should be noted.

Compliance with Modeled Policy Scenarios

This analysis assumes compliance with each of the modeled NAAQS policy scenarios. To the extent that these limitations are not adhered to, future ozone column conditions could be different.

Laboratory Techniques and Instrumentation

Additional uncertainty can be contributed by the laboratory techniques and instrumentation used for deriving the action spectra used to weight UV exposure. Discrepancies between the wavelengths of UV radiation intended to be administered and the wavelengths actually received by the test organism can result in orders of magnitude differences in the measured response. In

[7] Whether this recovery scenario, called "ozone superabundance," is likely to occur is open to debate, particularly because of the potential for complex interactions between global climate change and stratospheric ozone dynamics. Model computations have predicted both higher and lower amounts of ozone in the future.

addition, many action spectra are derived using monochromatic light sources that do not fully simulate the polychromatic light received directly from the sun.

Improvements in medical care/increased longevity

Improvements in medical care and predictions of increased longevity for many population subgroups could affect estimates of future skin cancer incidence and mortality significantly.

Changes in socioeconomic factors

Changes in socioeconomic factors (e.g., demographics and human behavioral changes) that could affect the accuracy of the analysis include:

- Changes in human UV exposure behavior: This evaluation assumes that human exposure behavior remains constant through time, and does not take into account innovations in sun protection technology (e.g., improved sunglasses and sunscreens), increased public awareness of the effects of overexposure to UV, and increased sensitization to the need for early treatment of suspicious lesions.

- Changes in socioeconomic profiles: Socioeconomic profiles can impact a variety of factors, ranging from demand for air travel to areas where high UV exposure is expected (i.e., the beach), to the types of skin cancer most commonly observed.

- Changes in population composition and size: Population composition changes such as the expected increase in Hispanic populations, whose more pigmented skin is thought to decrease skin cancer risk, could have significant effects on future U.S. skin cancer rates.

The above factors are either not easily quantified (e.g., human behavior; see Section 4.5.2. Behavioral Uncertainties), or they are not central to the analysis (e.g., improvements in medical care), and are therefore not addressed further in this evaluation.

Baseline Information

It is possible that error is introduced to the AHEF's results through misreporting of skin cancer incidence and mortality data (i.e., the AHEF's baseline estimates). With disease data, under-, over-, and misreporting are not uncommon. For example, a studies have revealed that the incidence of CMM has been systematically under-reported in the SEER data (Clegg et al. 2002).[8] The original SEER data indicated that CMM rates in white males were relatively flat or even falling (ranging from -11.1 percent to 3.3 percent annually after 1996). However, after adjusting for underreporting, CMM rates were actually found to have increased between 3.8 to 4.4 percent annually since 1981 (Clegg et al. 2002). Underreporting of CMM incidence is largely attributable to diagnosis in doctors' offices, as opposed to hospitals and other treatment centers with better reporting accuracy. However, the AHEF results are not significantly affected by this underreporting because CMM incidence estimates in the AHEF are not based directly on SEER incidence data. Rather, because the AHEF estimates CMM incidence based on the ratio of SEER

[8] There is little reason to believe that the SEER CMM incidence under-reporting extends to the NCI-based CMM mortality input information.

incidence data to projected annual mortality estimates, and because underreporting would affect both baseline and scenario estimates, the effects on incremental changes in CMM incidence would be second order.

1.15. Summary of Quantified and Unquantified Sources of Uncertainty

Of the major sources of uncertainty associated with the analysis, the total quantified uncertainty is roughly 32 percent, as summarized in Table 10.

Table 10: Major Sources of Quantified Uncertainty

Source of Uncertainty	Quantified Uncertainty
Translating column ozone to ground-level UV	
TUV Model	≈ 5 %
Translating UV exposure to human health effects	
Uncertainty in BAFs ▪ CMM mortality (3 %) ▪ NMSC mortality (4–7 %) ▪ NMSC incidence (30 %)	≤ 30 %
Early life exposure *versus* whole life exposure	≈ 10 %
Total $\sqrt{(5^2 + 30^2 + 10^2)}$	**≈ 32 %**

There are a variety of other unquantified sources of uncertainty that may contribute to overall analytical uncertainty associated with modeled ozone changes, changes in UV radiation, and changes in health effects. Table 11 summarizes the parameters that relate to these unquantified uncertainties.

Table 11: Factors with unknown contributions to uncertainty

Factor	Parameter
Changes in ozone estimates	Composition of future atmosphere
	Ability to model atmospheric processes accurately
	Response of tropospheric ozone to ozone layer recovery
	Effect of climate change
	Compliance with modeled NAAQS policy scenarios
Change in UV radiation estimates	Long-term systematic changes in atmospheric opacity (e.g., clouds, aerosols, other pollutants)
Change in health effect estimates	Changes in human UV exposure behavior
	Laboratory techniques and instrumentation for deriving an action spectrum
	Uncertainty with choice of action spectra
	Improvements in medical care/increased longevity
	Changes in socioeconomic factors (e.g., demographics and human behavioral changes)
	Baseline information (e.g., misreporting of skin cancer incidence and mortality data)
	Changes in population composition and size (including truncation of CMAQ model analysis area)

Accurate prediction of future changes in human health effects would require consideration of the net effect of all the factors described above. This challenge is beyond the ability of the current state of atmospheric and epidemiological science. In addition, direct measurements (e.g., of future UV levels or skin cancer incidence) cannot attribute explicitly observed changes to any specific factor, unless that factor is far more important than all the others combined. However, the principle of superposition can be used to examine the NAAQS impact (i.e., one effect in isolation) under the assumption that the other factors remain constant at current conditions. The validity of this principle is based on the assumption that the NAAQS impacts are independent of the other factors (e.g., behavioral changes will occur regardless of whether a new NAAQS standard is in place).

References

American Cancer Society: Cancer Facts and Figures 2007. Atlanta: American Cancer Society; 2007.

Bais, A., S. Madronich, J. Crawford, S. R. Hall, B. Mayer, M. VanWeele, J. Lenoble, J. G. Calvert, C. A. Cantrell, R. E. Shetter, A. Hofzumahaus, P. Koepke, P. S. Monks, G. Frost, R. McKenzie, N. Krotkov, A. Kylling, S. Lloyd, W. H. Swartz, G. Pfister, T. J. Martin, E.-P. Roeth, E. Griffioen, A. Ruggaber, M. Krol, A. Kraus, G. D. Edwards, M. Mueller, B. L. Lefer, P. Johnston, H. Schwander, D. Flittner, B. G. Gardiner, J. Barrick, R. Schmitt, International Photolysis Frequency Measurement and Model Intercomparison: Spectral actinic solar flux measurements and modeling, *J. Geophys. Res.*, 108, 8543, doi:1029/2002/JD002891, 2003.

Bruhl, C. and P. J. Crutzen , On the disproportionate role of tropospheric ozone as a filter against solar UV-B radiation, *Geophys. Res. Lett.*, 16, 703-706, 1989.

Chen J.G., A. B. Fleischer, Jr, E. D. Smith, .C. Kancler, N. D. Goldman, P.M. Williford, S. R. Feldman. Cost of nonmelanoma skin cancer treatment in the United States. *Dermatol Surg.* 2001; 27(12): 1035-8

Cokkinides VE, Johnston-Davis K, Weinstock M, O'Connell MC, Kalsbeek W, Thun MJ, Wingo PA. Sun exposure and sun-protection behaviors and attitudes among US youth 11 to 18 years of age. Preventive Medicine, 2001, 33:141-151.

de Gruijl F.R. and J.C. van der Leun, Estimate of the wavelength dependency of ultraviolet carcinogenesis and its relevance to the risk assessment of a stratospheric ozone depletion, *Health Phys*,. **4**, 317–323, 1994.

de Gruijl, F.R. and P.D. Forbes (1995), "UV-induced skin cancer in a hairless mouse model," *BioEssays* 17:651-660.

Eder, B, and S. Yu (2006). A performance evaluation of the 2004 release of Model-3 CMAQ. Atmospheric Environment 40(26):4811–4824.

Godar DE, Urbach F, Gasparro FP, van der Leun JC. UV doses of young adults. Photochemistry and Photobiology, 2003, 77(4):43-457.

Joseph, J. H., W. J. Wiscombe and J. A. Weinman, The delta-Eddington approximation for radiative flux transfer, *J. Atmos. Sci.* **33**, 2452-2459, 1976.

Koepke et al., Comparison of models used for UV Index calculations, Photochemistry and Photobiology, 67 (6) 657-662, 1998.

Kyle JW, Hammitt JK, Lim HW, Geller AC, Hall-Jordan LH, Maibach EW, De Fabo EC, Wagner MC. Economic Evaluation of the U.S. Environmental Protection Agency's SunWise Program: Sun Protection Education for Young Children. Forthcoming in Pediatrics Electronic Pages, May 2008.

Longstreth J.D. (1998), "Melanoma genesis: putative causes and possible mechanisms," in *Cutaneous Melanoma*, C.M. Balch, A.N. Houghton, A.J. Sober, and S-J. Soong (eds.), St. Louis: Quality Medical Publishing, Inc.

Madronich, S. and F. R. de Gruijl (1994), "Stratospheric ozone depletion between 1979 and 1992: Implications for biologically-active ultraviolet-B radiation and non-melanoma skin cancer incidence," Photochemistry and Photobiology 59:541-546.

Madronich, S. and G. Weller, Numerical integration errors in calculated tropospheric photodissociation rate coefficients, J. Atmos. Chem., 10, 289-300, 1990.

Madronich, S. and S. Flocke. The role of solar radiation in atmospheric chemistry. In *Handbook of Environmental Chemistry, Volume 2 Part L: Environmental Photochemistry* (Edited by P. Boule), pp. 1-26. Springer-Verlag, Heidelberg, 1999.

Madronich, S., R. E. McKenzie, L. O Björn, and M. M. Caldwell, Changes in biologically active ultraviolet radiation reaching the Earth's surface, in *Environmental Effects of Stratospheric Ozone Depletion* - 1998 Update (J. van der Leun, M. Tevini, and X. Tang, eds.), United Nations Environmental Programme, Nairobi, November 1998.

Madronich, S. (1999). Some comments on the methods used to estimate the effects of HSCTs on atmospheric ozone, surface UV radiation, and skin cancer incidence. Paper presented at a workshop held by EPA, "Meeting on Next Generational Supersonic Transport Risk Assessment Methods," November 18–19, 1999 at ICF Consulting, Washington, DC.

Matthews, T.J. and B.E. Hamilton. (2005). Trend Analysis the Sex Ratio at Birth in the United States. *National Vital Statistics Reports 53:20.* Available online at: http://www.cdc.gov/nchs/data/nvsr/nvsr53/nvsr53_20.pdf

McKinlay, A. F. and Diffey, B. L., A reference action spectrum for ultraviolet induced erythema in human skin. In *Human Exposure to Ultraviolet Radiation: Risks and Regulations* (Edited by W. R. Passchier and B. F. M. Bosnjakovic), pp. 83-87. Elsevier, Amsterdam, 1987.

Mrozek, J.R., and L.O. Taylor. 2002. "What Determines the Value of Life? A Meta-Analysis." Journal of Policy Analysis and Management 21(2):253-270.

Nack, M. L. and A. E. S. Green, Influence of clouds, haze, and smog on the middle ultraviolet reaching the ground., 12, 2405-2415, 1974.

National Center for Health Statistics (2007). *Bridged-race Vintage 2006 Postcensal Population Estimates for July 1, 2000–July 1, 2006*. Available online at: http://www.cdc.gov/nchs/about/major/dvs/popbridge/datadoc.htm

Petropavlovskikh, I. *Evaluation of Photodissociation Coefficient Calculations for Use in Atmospheric Chemical Models*, Ph.D. thesis, U. of Brussels/NCAR Cooperative Thesis No. 159, National Center for Atmospheric Research, Boulder, 1995.

Pitcher, H.M., and J.D. Longstreth (1991), "Melanoma mortality and exposure to ultraviolet radiation: An empirical relationship," Environment International 17:7-21.

Toon, O. B., C. P. McKay, T. P. Ackerman, and K. Santhanam, *J. Geophys. Res.*, **94**, 16287, 1989.

U.S. Bureau of Labor Statistics, Department of Labor. Occupational Employment Statistics (OES) Survey: May 2005 National OES Estimates. [cited 2007 Dec 26]. Available from: http://www.bls.gov/oes/.

U.S. Census Bureau (2000). *Component Assumptions of the Resident Population by Age, Sex, Race, and Hispanic Origin*. Available online at: http://www.census.gov/population/www/projections/natdet-D5.html

U.S. Census Bureau (2005). *State Interim Population Projections by Age and Sex: 2004–2030*. Available online at: http://www.census.gov/population/www/projections/projectionsagesex.html

U.S. Environmental Protection Agency. EPA Guidelines for Preparing Economic Analyses. Washington, DC: Office of the Administrator, U.S. Environmental Protection Agency; 2001. Report No. 240-R-00-003.

U.S. EPA (2003). Human Health Benefits of Stratospheric Ozone Protection. Global Programs Division, Office of Air and Radiation, U.S. EPA, Washington, DC.

U.S. EPA and NASA (2001). Human Health Effects of Ozone Depletion From Stratospheric Aircraft. U.S. EPA, Washington, DC

U.S. EPA (2008). Personal communication.

U.S. Environmental Protection Agency. Regulatory Impact Analysis: Protection of Stratospheric Ozone, E. Final Report. 1988.

USSA, *US Standard Atmosphere* National Oceanic and Atmospheric Administration, National Aeronautics and Space Administration, United States Air Force, Washington D.C., 1976.

Viscusi, V.K., and J.E. Aldy. 2003. "The Value of a Statistical Life: A Critical Review of Market Estimates Throughout the World." Journal of Risk and Uncertainty 27(1):5-76.

Appendix A: Ground Level SCUP-h UV with 70 and 84 ppb by Day

This Appendix will provide a series of maps showing ground level SCUP-h UV levels under 70 and 84 ppb NAAQS for ozone for several specific days in the summer months – June 1, June 20, July 1, and August 1.

Figure A-1: Ground Level SCUP UV, June 1; 70 ppb Scenario

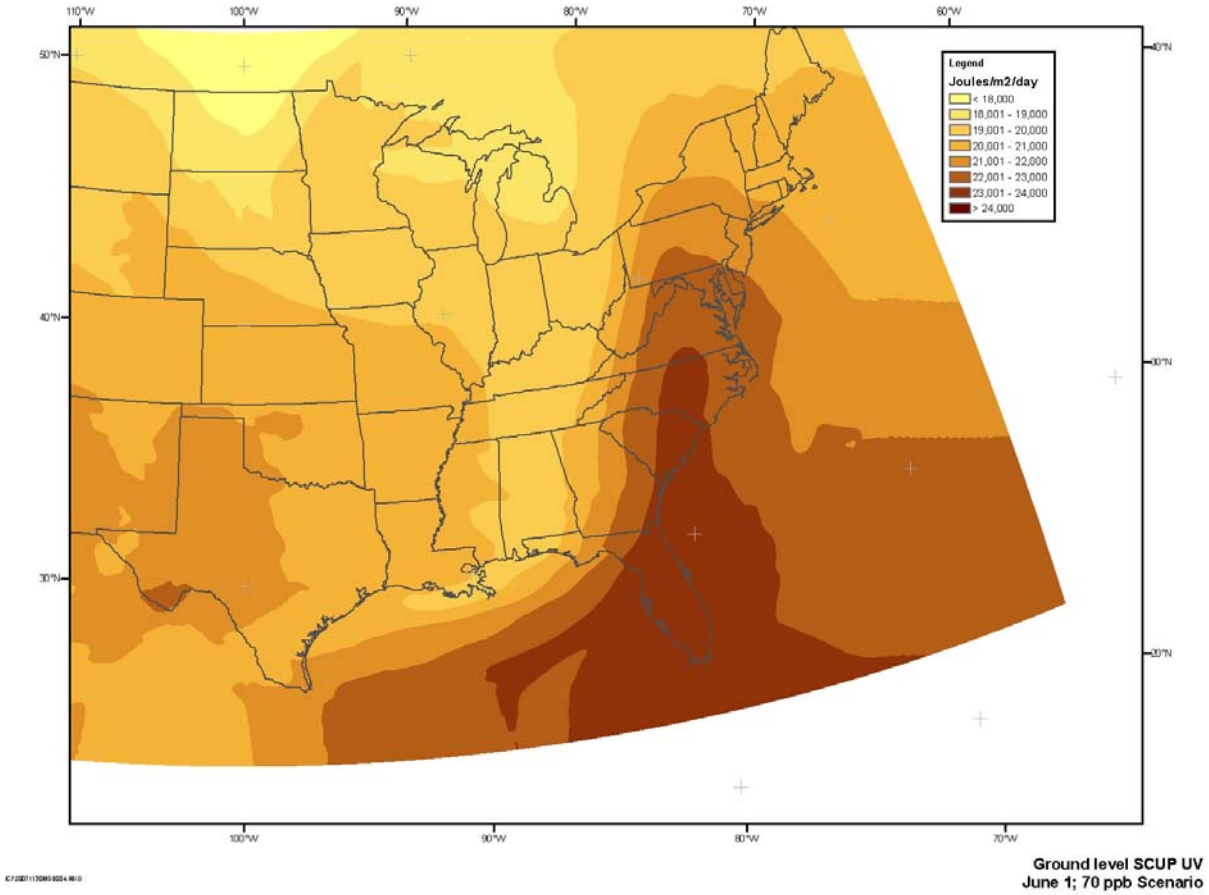

Figure A-2: Ground Level SCUP UV, June 1; 84 ppb Scenario

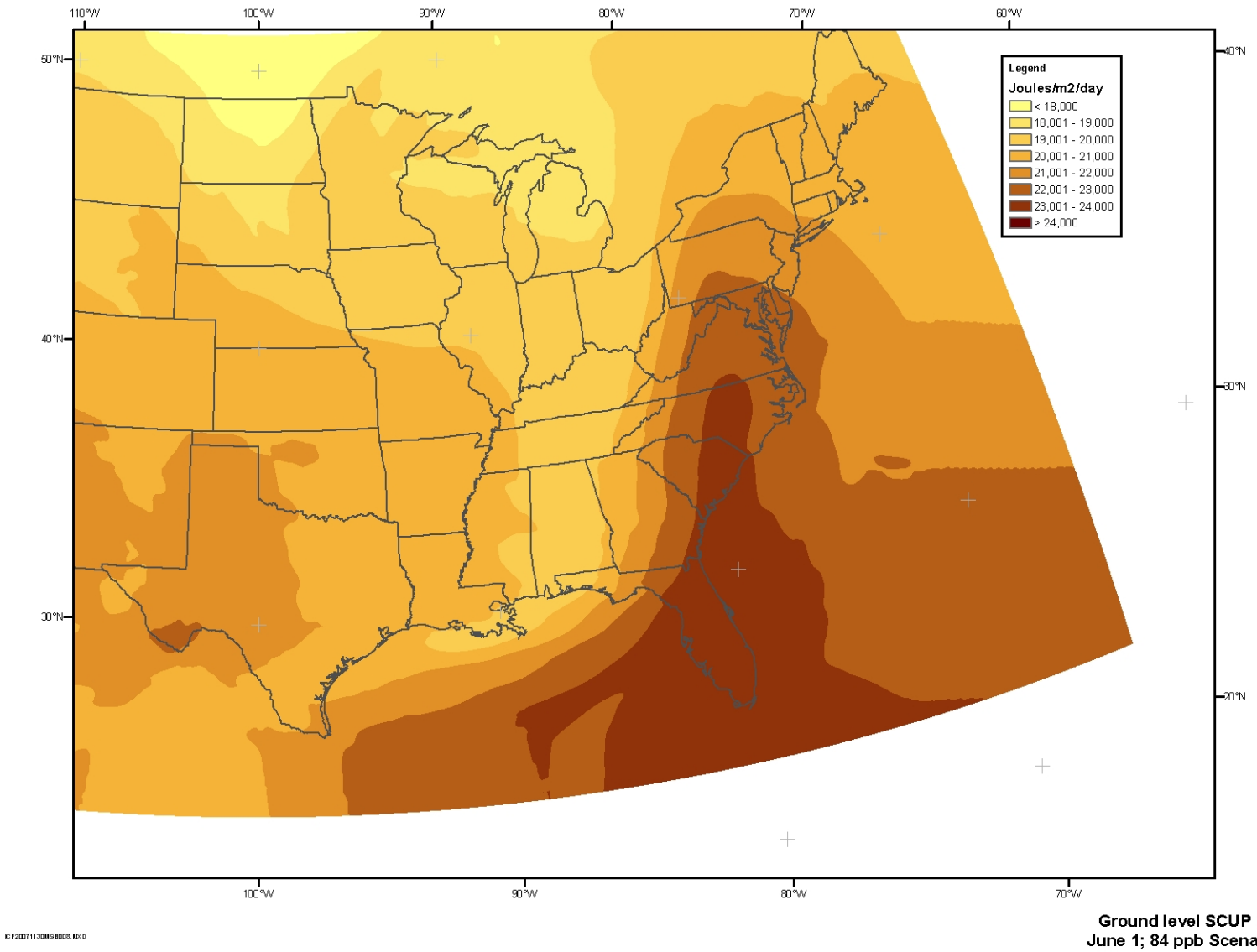

Figure A-3: Ground Level SCUP UV, June 20; 70 ppb Scenario

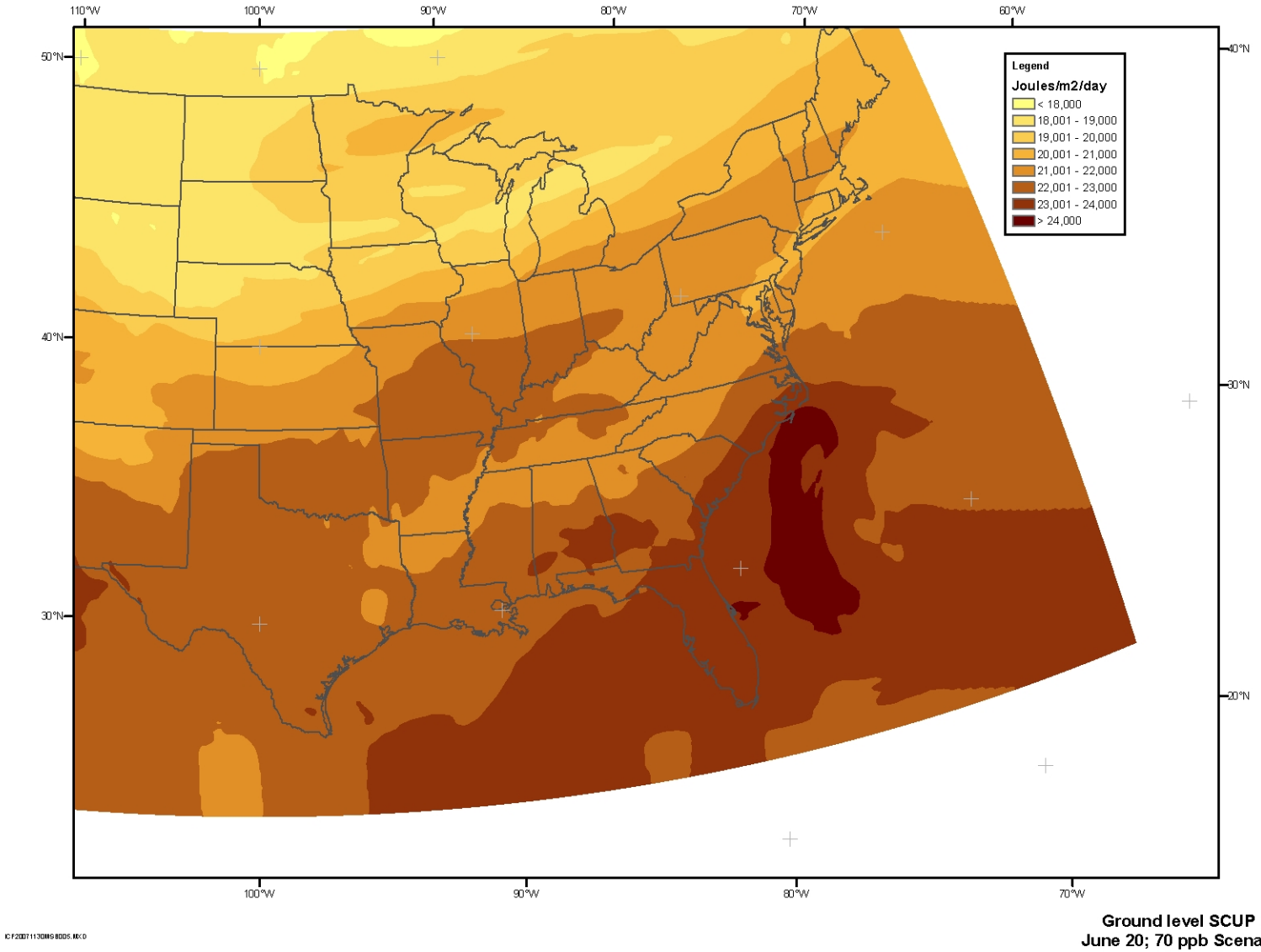

Figure A-4: Ground Level SCUP UV, June 20; 84 ppb Scenario

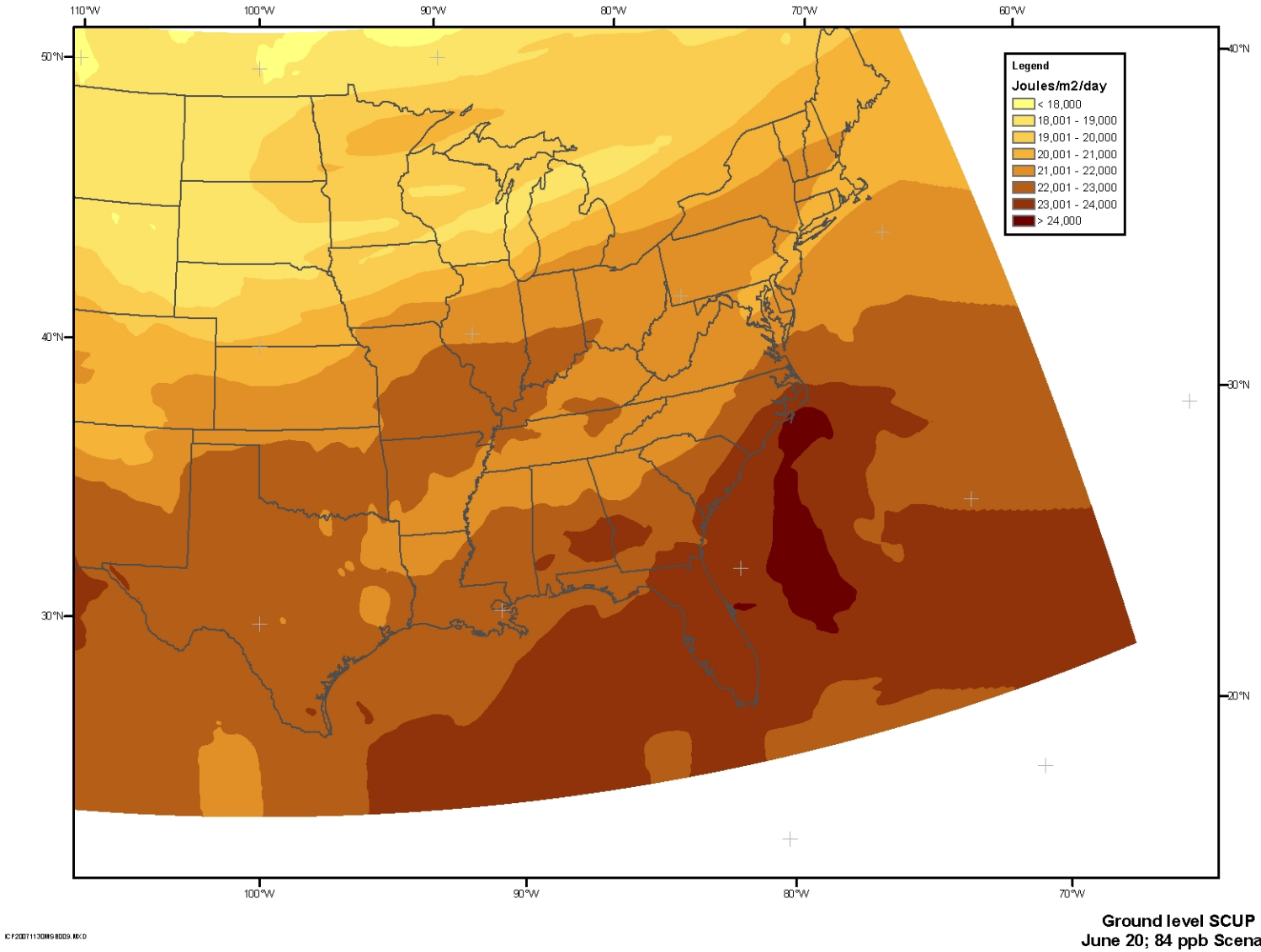

Figure A-5: Ground Level SCUP UV, July 1; 70 ppb Scenario

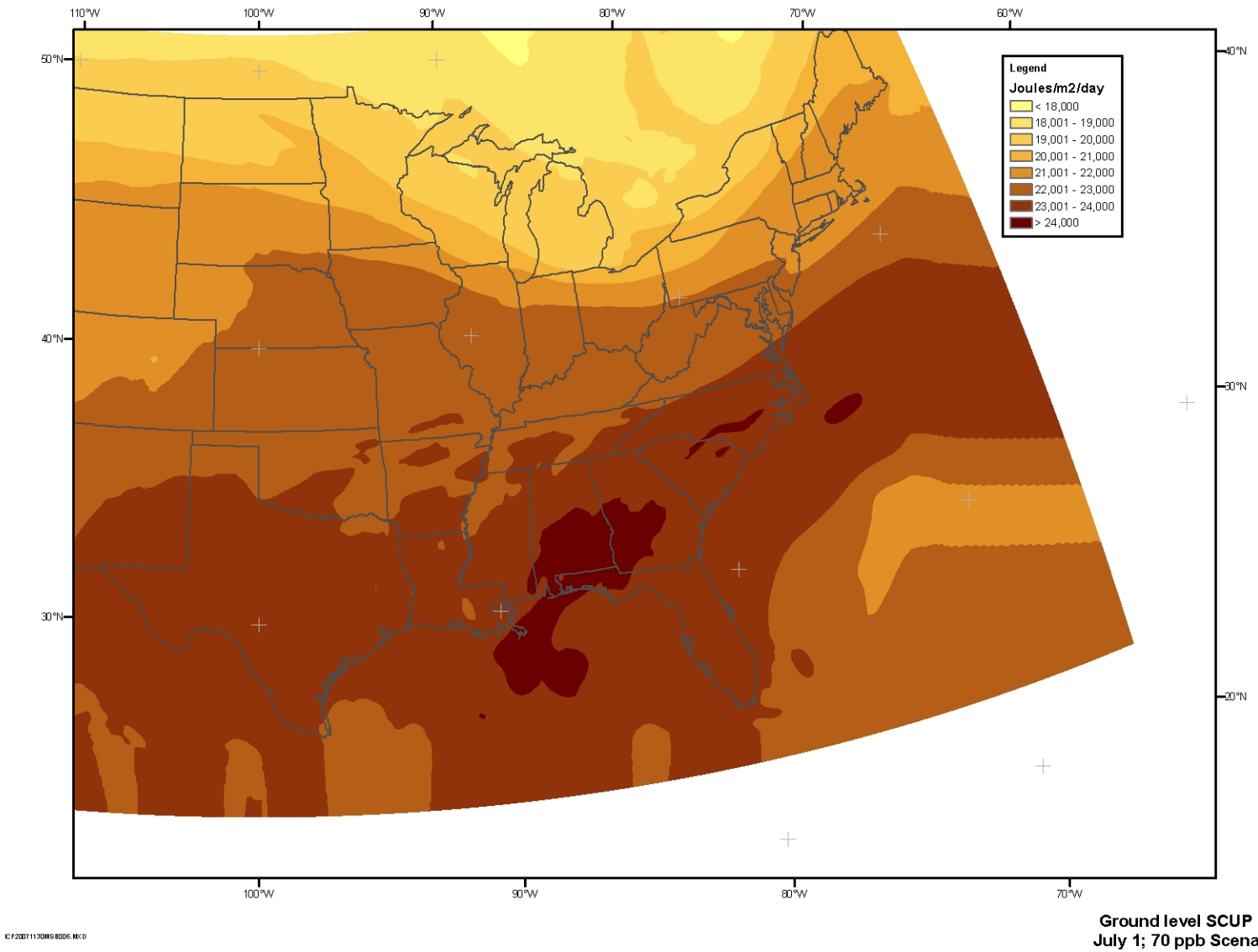

Figure A-6: Ground Level SCUP UV, July 1; 85 ppb Scenario

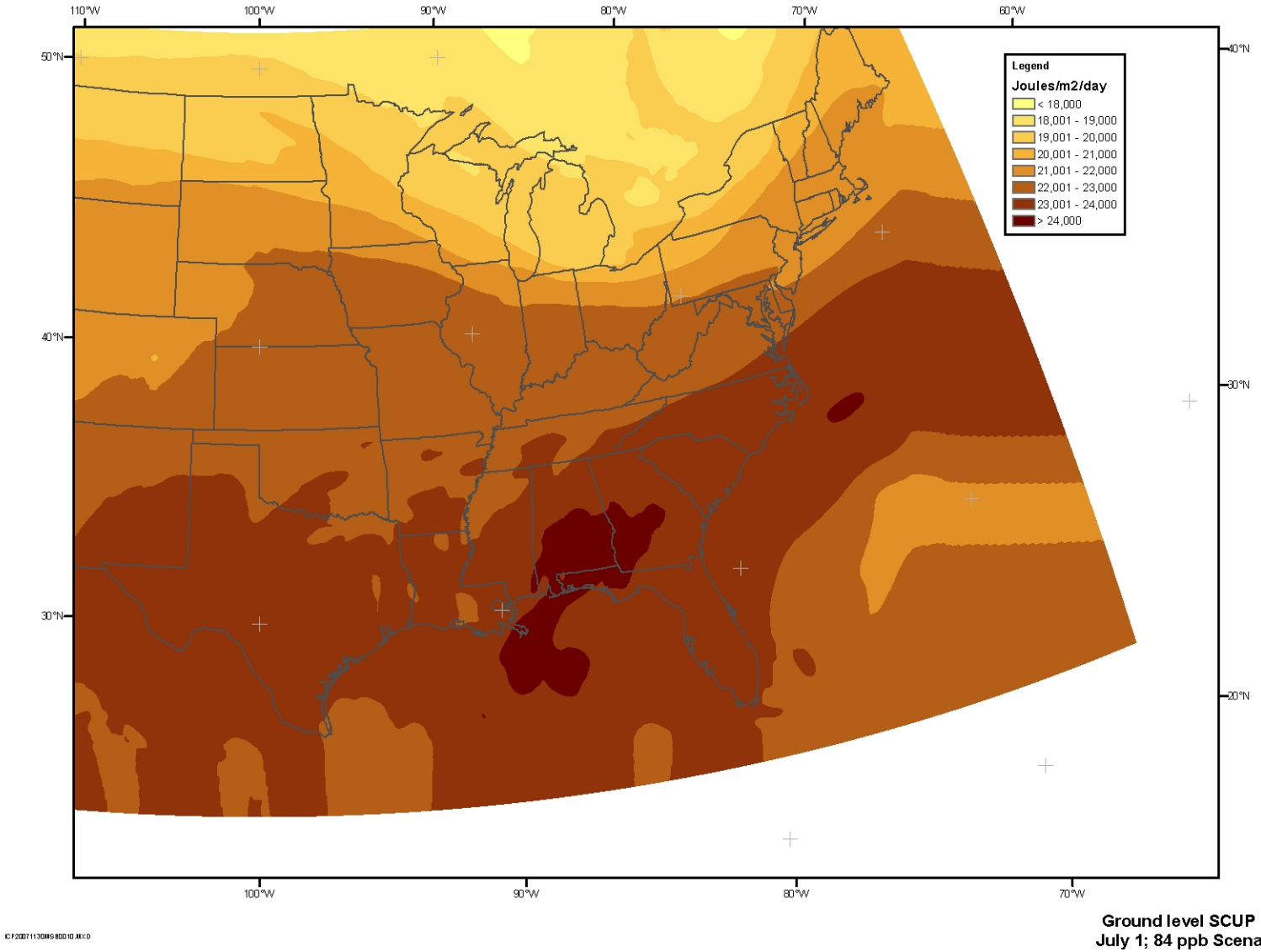

Figure A-7: Ground Level SCUP UV, August 1; 70 ppb Scenario

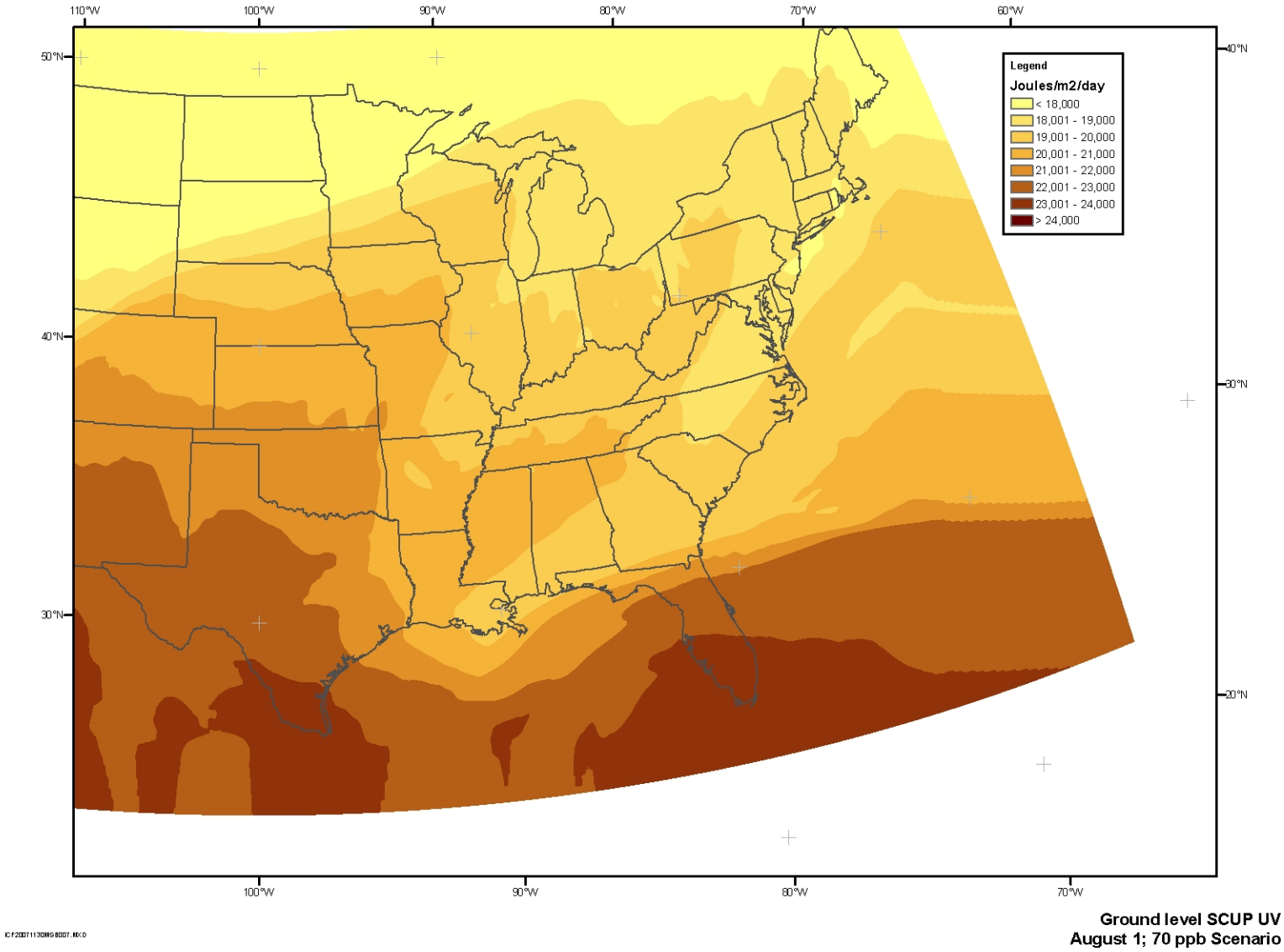

Figure A-8: Ground Level SCUP UV, August 1; 84 ppb Scenario

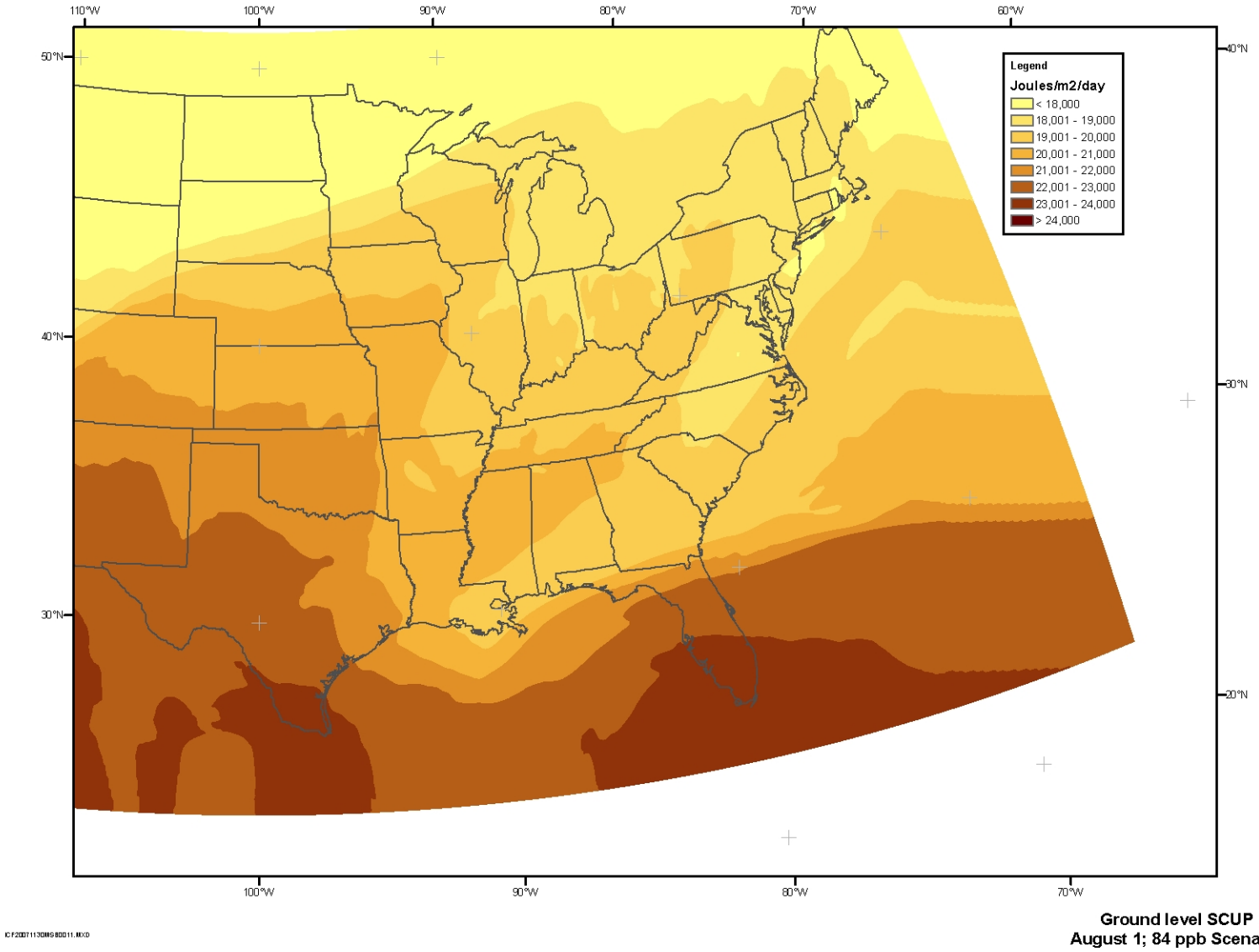

Appendix B: Overview of Evaluation Methodology

The schematic presented below provides a graphical summary of the method used in this evaluation. Atmospheric inputs to the process are listed along the left-hand side and the various process stages are described along the bottom.

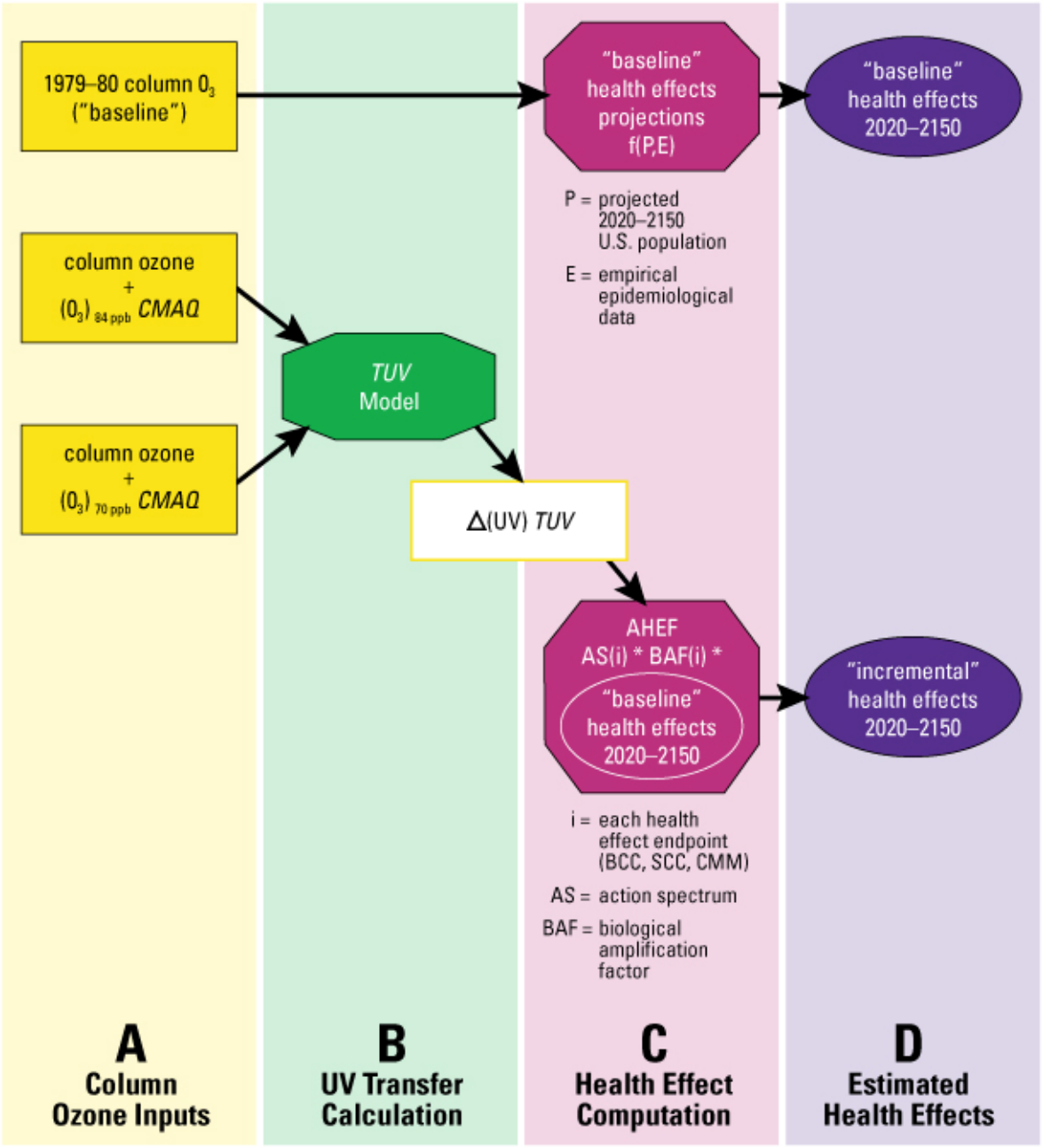

Glossary

AHEF	Atmospheric and Health Effects Framework
BAF	Biological Amplification Factor
BAU	Business as Usual
BCC	Basal Cell Carcinoma
BLS	Bureau of Labor Statistics
CDC	Centers for Disease Control and Prevention
CMAQ	Community Multiscale Air Quality
CMM	Cutaneous Malignant Melanoma
DU	Dobson Units
EPA	United States Environmental Protection Agency
NAAQS	National Ambient Air Quality Standard
NCEE	National Center for Environmental Economics
NCI	National Cancer Institute
OAR	Office of Air and Radiation
SCC	Squamous Cell Carcinoma
SCUP-h	Skin Cancer Utrecht-Philadelphia-human
sza	solar zenith angle
TOCOR	Task Order Contracting Representative
USSA	United States Standard Atmosphere